National   Défense
Defence   nationale

AD-A205 404

A STATISTICAL ANALYSIS OF THE OUTPUT SIGNALS
OF AN ACOUSTO-OPTIC SPECTRUM ANALYZER
FOR CW SIGNALS

by

Guy J. Farley

DEFENCE RESEARCH ESTABLISHMENT OTTAWA
REPORT NO. 993

Canada

October 1988
Ottawa

89   3   01   087

A STATISTICAL ANALYSIS OF THE OUTPUT SIGNALS OF AN ACOUSTO-OPTIC SPECTRUM ANALYZER FOR CW SIGNALS

by

Guy J. Farley
Radar ESM Section
Electronic Warfare Division

ABSTRACT

A statistical analysis of the output signals of an acousto-optic spectrum analyzer (AOSA) is performed for the case when the input signal is a continuous-wave (CW). To this end, a statistical model of these output signals is presented as a basis for the different analyses along with some numerical algorithms to calculate the deterministic components on a digital computer.

Using this model, the optimum test for the detection of a known frequency is derived and its performance is analyzed. To deal with the unknown frequency situation, a scheme which is easily implemented with a finite impulse response (FIR) filter is presented and its performance degradation as compared to the case of a known frequency is analyzed.

The frequency estimation problem is also analyzed and the Cramér-Rao lower bound on the variance of any unbiased estimator is calculated. Since the Cramér-Rao bound indicates that any unbiased estimator would exhibit undesirable characteristics, the performance of the peak-detecting estimator is analyzed. It is shown that this latter estimator is biased but has the desired characteristic of having a zero average bias.

Finally, the power estimation problem is analyzed under the assumption that the frequency of the input signal is known. Under this assumption, it is found that the maximum likelihood (ML) estimator is an *efficient* estimator which means that its variance is the lowest possible variance of any unbiased estimator. The effects of inaccuracies in the frequency assumption on the performance of the ML estimator are also analyzed.

RÉSUMÉ

Une analyse statistique des signaux générés par un analyseur de spectre acousto-optique est effectuée pour des ondes continues. À cette fin, on présente un modèle statistique des signaux servant de base aux différentes analyses ainsi que des algorithmes pour le calcul des signaux en l'absence de bruit.

En utilisant ce modèle, on obtient le test décisionnel optimale pour la détection d'un signal dont la fréquence est connue et on analyse sa performance. Pour traiter du cas dont la fréquence est inconnue, on présente une solution qui est facilement exécutée par un filtre digital dont la réponse à une impulsion est finie et on analyse sa performance dégradée par rapport au cas dont la fréquence est connue.

Le problème de l'estimation de la fréquence est également analysé et la limite Cramér-Rao pour la variance minimale d'une estimation non-biaisée est calculée. Compte tenu des charactéristiques indésirables d'une estimation non-biaisée mises en lumière par la limite Cramér-Rao, on calcule la performance de l'estimation qui consiste à détecter le pic. On démontre que cette dernière estimation est biaisée mais qu'elle a l'heureuse charactéristique d'un biais moyen nul.

En dernier lieu, le problème de l'estimation de la puissance est analysé en assumant que la fréquence du signal soit connue. Pour ce dernier cas où la fréquence est connue, on démontre que l'estimation à probabilité maximale est *efficiente,* ce qui veut dire que la variance de cette estimation non-biaisée est minimale par rapport à n'importe laquelle des estimations non-biaisées. Les effets de l'inexactitude de notre connaissance de la fréquence sur la performance de l'estimation à probabilité maximale sont également analysés.

EXECUTIVE SUMMARY

DREO is investigating the use of Bragg cell receivers for the development of Radar Electronic Support Measures (RESM) systems for the armed forces. Perhaps the most mature Bragg cell receiver at the present is the one-dimensional configuration which has come to be commonly known as the acousto-optic spectrum analyzer (AOSA). In this report, we are concerned with the processing of the output signals from an AOSA for the case when the input signal is a continuous-wave (CW).

To this end, we present a statistical model of the system along with some numerical algorithms to calculate the outputs on a digital computer. Using this model, we obtain a detection algorithm which is easily implemented and we also characterize its performance. Next, we consider the frequency estimation problem and we show that an estimator of any significance would have to be biased especially for certain system configurations. In order to provide a viable solution to the frequency estimation problem, we propose the peak-detecting algorithm and we characterize its performance. Finally, we consider the power estimation problem and we show that the maximum-likelihood (ML) estimator is optimum when the frequency estimate is accurate and we also analyze the effects of inaccuracies in the frequency estimate on the performance of the ML estimator.

This report is a major step in the development of post-processing algorithms for the AOSA. Although we have confined our analysis to the case of CW signals, the derivations could be applied to other signal types and system configurations. This report contributes to a better understanding of the critical issues and tradeoffs that are involved and in this way provides a basis for the development of an optimal or suboptimal solution to the general problem which is more complex.

TABLE OF CONTENTS

LIST OF FIGURES

LIST OF TABLES

xi

1.0 INTRODUCTION

1.1 Background

Over the last century, electronic systems have grown to predominance in the command, control and communications area of military logistics. Besides the development of communications and radar systems for military applications, the desire to disrupt the enemy's electronic systems has fostered the development of a new area called *electronic warfare* (EW). The purpose of EW is to make use of electromagnetic energy to determine, exploit, reduce or prevent the enemy's use of the electromagnetic spectrum, while insuring the friendly use of this spectrum. In electronic warfare applications, receivers can be used to intercept signals from enemy transmitters, while jamming transmitters are used to generate false information or noise to modify the signal received by the enemy. The intercepted information could be used to identify and evaluate the threat associated with an emitter or to detect the parameters of the transmitter which would help in a jamming operation. In this context, although some information on the transmitter is available, the transmitter parameters cannot be used in the design of the receiver since the radiating sources are noncooperative. Under such conditions, the intercepting receiver must be designed somewhat independently of the transmitter so that it is able to receive a variety of different signals and extract the desired information. For that reason, the design of such receivers is complex and requires a good understanding of the signal environment in which the receiver must operate.

Microwave electronic warfare receivers for this kind of operation can be divided into the following groups according to their structures: crystal video receivers, superheterodyne ("superhet") receivers, instantaneous frequency measurement (IFM) receivers, channelized receivers, compressive (also called microscan) receivers, and Bragg cell receivers. For electronic warfare applications, the performance of the latter three types of receivers is expected to be far better than that of the former three types in terms of the width of the spectrum that can be dealt with, the signal levels that could be sucessfully intercepted and the number of signals that could be simultaneously dealt with by the receiver [1, pp. 3]. The full potential of these receivers has not yet been reached due to various technical difficulties and most of the research and development presently underway in this area is aimed at overcoming these difficulties.

1.2 Acousto-Optic Spectrum Analyzer

In this report, we will solely be concerned with the most mature Bragg cell receiver configuration which has come to be commonly called an *acousto-optic spectrum analyzer* (AOSA). In this receiver, input electrical radio frequency (RF) signals are first transformed into spatial patterns which modulate a light beam, generating a spatial distribution of the light intensity which is sensed by a photodetector array. This spatial distribution depends on the parameters of the signals received and can be used to discern the needed information. While many modulation techniques can be used in optical processors (e.g., thermo-plastic deformation and electro-optic modulation), Bragg cell receivers use acousto-optic modulation. In this case, the electrical signal is converted into an acoustic wave which propagates through an optically transparent material (Bragg cell). Through the elasto-optic effect, the acoustic wave produces a spatial modulation of the refractive index in the Bragg cell. When a coherent light wave is passed through the Bragg cell, the refractive index modulation (and hence the electric signal waveform) is impressed onto the optical wavefront as a spatial phase modulation. A suitable optical lens system is used to convert the modulated optical wavefront into a spatial intensity modulation corresponding to the power spectrum of the Bragg cell input signal. The transformed signal is read and converted back to electrical form using a linear array of photodetectors. Since each photodetector, due to its physical size, provides an output which is proportional to the integral of the spectrum over a narrow portion, we can describe the AOSA as a form of channelized receiver.

Although the principles discussed above have been known for many years, it was only fairly recently that the requisite technologies have become sufficiently developed to make Bragg cell optical processors feasible. Of particular importance is the development of lasers with adequate output levels since high intensity in the optical wave is essential to achieve satisfactory performance. Other significant technological advances over the last decade include the achievement of large (> 100) time-bandwidth products in Bragg cells and the development of large photodetector arrays. While much work remains to be done, especially in the areas of dynamic range and output rate of detector arrays, these recent developments in optical processor technology have encouraged the exploration of Bragg cell processors for microwave receiver applications.

The most attractive aspect of using the Bragg cell as a microwave receiver is its potentially extremely small size and low cost. Theoretically, a Bragg cell receiver can perform as a conventional channelized receiver without the hundreds of filters required in such a receiver. The Bragg cell receiver can have a maximum time-bandwidth product of approximately 1000 which is equivalent to a channelized receiver with 1000 filters. [1, pp. 150]. Furthermore, the development of integrated optical circuits (IOCs) makes the integration of the laser source, the Bragg cell transducer, output detector arrays, and the optical lens system on a single chip possible. An integrated optical Bragg cell receiver could have a volume as small as $0.1 \times 2 \times 6$ cm^3 [2]. These developments make the Bragg cell approach the most attractive electronic warfare receiver for airborne applications [1, pp. 150].

1.3 Problem Statement and Report Organization

In this report, we are concerned with the problem of processing the output signals of an AOSA when this receiver is used to monitor the electromagnetic environment in an effort to detect the presence of radar signals and measure their respective parameters. Such EW receivers must be able to cope simultaneously with many different radar signals. In addition to radar, other types of signals may be present including beacons and transponders, jammers, missile guidance signals, data signals, altimeter signals, navigation emissions, and identification friend or foe (IFF) signals [3, pp. 1]. This means that there is a large variety of signals that we can expect to intercept. Since a statistical analysis dealing with all of these signals at once would be extremely complex and likely intractable, we will limit our analysis to the case when we are receiving continuous-wave (CW) signals. In the case of a CW signal, once we have detected its presence, there are two parameters that we are interested in estimating: its frequency and its power. We feel that this is a good place to start as it will contribute to a better understanding of the critical issues and tradeoffs and provide a more rigorous and systematic foundation upon which optimal or suboptimal algorithms can be derived for the solution of the whole problem. We will therefore address the problem of finding efficient algorithms for the processing of the outputs of an AOSA in order to fulfill the tasks of detecting the presence of CW signals and estimating their respective frequency and power.

To begin the analysis of this problem, we present in section 2.0 a statistical model of the output signals from an AOSA which will form the basis of the statistical analyses performed in the subsequent sections. Using this model, we then consider the detection problem in section 3.0, the frequency estimation problem in section 4.0, and the power estimation problem in section 5.0. Finally, in section 6.0 we summarize the results and discuss the needs for further research.

2.0 THE SYSTEM MODEL

2.1 Introduction

In order to perform a statistical analysis of the performance of any given system, we must first obtain a mathematical model of the signals and the noise for that system. In this section, we present a model for the signals and the noise at the output of an acousto-optic spectrum analyzer (AOSA). This section is fundamental to this report as all the following sections will be based on it. Indeed, the detection, frequency estimation and power estimation analyses performed in the subsequent sections will be based on the model presented in this section.

In the next subsection, we present a model for the signals at the output of an AOSA assuming the noiseless situation. To this end, we present the AOSA configuration that will be analyzed in this report along with a first-order theory of operation. Next,

we present a mathematical model that can be used to represent the signals and we give some numerical algorithms that can be used to calculate the outputs on a digital computer.

In the third subsection of this section, we give the noise model that will be used in this report along with a discussion of why it was chosen. Finally, in the last subsection of this section we conclude by giving the complete signal plus noise model that will be used in the subsequent sections for the different statistical analyses.

2.2 Signal Model

2.2.1 AOSA Configuration

A block diagram of the AOSA configuration of interest in this report is shown in Figure 1. The first component of this system is the laser which is the source of the optical wave. Since the beam provided by the laser is usually relatively small, a beam expander is required so that a plane wave commensurate with the physical size of the Bragg cell is obtained. This is usually accomplished with a series of lenses which are also used to improve the quality of the light in terms of getting a plane optical wave.

The key component of this system is the Bragg cell which acts as an input device by transforming the input electrical signal into an acoustic wave that propagates in a transparent medium and therefore interacts with the optical wave. The phenomenon by which this interaction takes place is called *acousto-optic diffraction.* The mechanism through which acousto-optic diffraction takes place is due to the fact that when an acoustic wave propagates in a transparent medium, it induces localized refractive index variations via the elasto-optical effect. The acoustic wave acts like a moving phase grating which may diffract portions of an incident light beam into one or more beams which are referred to as the different diffracted orders. Provided the Bragg cell is tilted by the proper angle θ_B (the Bragg angle) then it is possible to obtain only one diffracted order. The proper value for θ_B depends on the frequency of the optical wave and the frequency of the acoustic wave. (The reader in search of an intuitive understanding of acousto-optic diffraction can consult [4], while a more rigorous derivation from the fundamental Maxwell's equations is given in [5].) An important characteristic of acousto-optic diffraction is that the diffracted light wave will be phase modulated by the phase of the acoustic wave with the result that it will be diffracted at an angle directly proportional to the frequency of the acoustic wave. The Fourier transform lens will then map the two-dimensional Fourier transform of this diffracted wave onto its focal plane. For that reason, we will henceforth refer to this plane as *the frequency plane* . (The reader who desires an understanding of how a lens can perform a two-dimensional Fourier transform can consult [6, pp. 77-87].) Since we assume that the incident optical wave to the Bragg cell and the acoustic wave in the cell are both plane waves, then one dimension of the frequency plane will simply be the one-dimensional Fourier transform
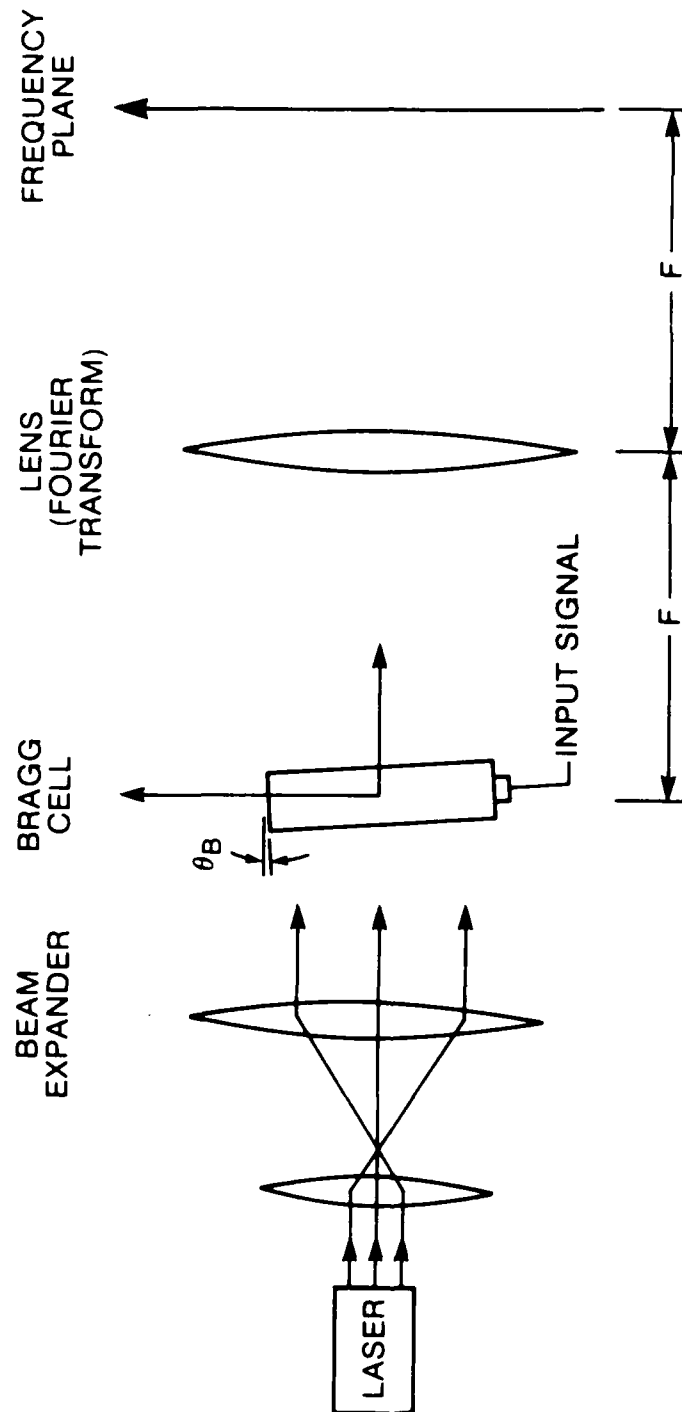
FIGURE 1: ACOUSTO-OPTIC SPECTRUM ANALYZER CONFIGURATION

of the input signal and this will be the same as we move along the other dimension of the frequency plane.

In order to convert the result of this optical processing to electrical form, we place a linear array of photodetectors in the frequency plane (which is the focal plane of the Fourier transform lens). These photodetectors perform a spatial averaging of the light intensity which represents the power spectrum of the input signal. In this report, we will also assume that these photodetectors are of the time-integrating type. This is a reasonable assumption as many practical devices operate in that way, which means that they periodically integrate, sample and dump the light intensity (the power spectrum of the input signal).

2.2.2   Mathematical Model

From the standpoint of the above description concerning the AOSA configuration of interest in this report, we will now proceed to do a step by step derivation of a mathematical model that is often used to calculate its output signals. Using this approach, we will introduce some additional practical issues and show how these are incorporated in the model.

As a starting point, if $u(t)$ is the input signal, then its Fourier transform is

$$U(\omega) = \int_{-\infty}^{\infty} u(t) \exp(-i2\pi f t) dt.$$

Now, any physical Bragg cell would have a finite size and it is clear that the light in the frequency plane can only represent the spectrum analysis of that portion of the signal which has not entirely propagated through the Bragg cell at the particular point in time. In effect, this means that the AOSA has a finite time aperture over which to perform spectrum analysis and this determines its fundamental limit in spectral resolution. To account for this, we can model the amplitude and phase of the light wave in the frequency plane as a sliding window spectrum which for a given time t is

$$\int_{-\infty}^{\infty} w(\beta) u(t - \beta) \exp(-i2\pi f \beta) d\beta$$

where $w(\beta)$ is a rectangular function to account for the fact that the Bragg cell has a finite size and hence the input signal $u(t)$ will appear to experience truncation in time.

It turns out that this window function $w(\beta)$ can also be used to account for some other practical issues concerning the Bragg cell and the laser beam. For instance, the window function can be used to account for the fact that the acoustic wave will be attenuated as it propagates in the cell. We usually account for this by changing $w(\beta)$

from a rectangular function to a truncated exponential decaying function. The extent to which it will be important to account for this attenuation of the acoustic wave as it propagates through the cell will depend on the Bragg cell, the frequency band and the specific system design that is used.

Still another practical issue that the window function $w(\beta)$ is able to incorporate is the uniformity of illumination on the Bragg cell. Most practical lasers have a Gaussian shaped profile and this fact can be used to obtain a windowed spectrum analysis with lower sidelobes. This effect can be incorporated in the model through the function $w(\beta)$ to which we add a Gaussian component. The extent to which it will be important to account for this practical issue will depend on the laser and the specific system design that is used.

Yet another component of our AOSA system which will affect our mathematical model is the linear array of photodetectors that we use. First, we should note that these photodetectors are sensitive to the light intensity which corresponds to the squared magnitude of the optical wave. Hence, in our model we will use a sliding window power spectrum which for a given time t is

$$\left| \int_{-\infty}^{\infty} w(\beta) u(t - \beta) \exp(-i2\pi f \beta) d\beta \right|^2 .$$

Secondly, we should note that the array does not contain an infinite number of photodetectors and nor are these of infinitesimal size. Since the photodetectors have a certain width, they will spatially integrate the light intensity which corresponds to a frequency integration of the power spectrum of the input signal. We can therefore represent the output of an individual photodetector as

$$\int_{-\infty}^{\infty} H(f - f_k) \left| \int_{-\infty}^{\infty} w(\beta) u(t - \beta) \exp(-i2\pi f \beta) d\beta \right|^2 df$$

where $H(f)$ describes the spatial response of that photodetector. Usually, it is assumed that $H(f)$ is a rectangular function and the bandwidth that it represents is analogous to the bandwidth of a filter in a channelized receiver. However, if we know which array of photodetectors will be used and there is some data available concerning the profile of the individual detector elements, then $H(f)$ can be used to take this into account. The frequency that corresponds to the center of a photodetector element is called f_k and we will sometimes refer to that frequency as *the frequency associated with the kth detector.*

Thirdly, as we mentioned earlier, we will assume in this report that the photodetectors are of the time-integrating type. In that case, we get that the ouput of an individual photodetector can be represented as

$$\int_{jI}^{(j+1)I} \int_{-\infty}^{\infty} H(f - f_k) \left| \int_{-\infty}^{\infty} w(\beta) u(t - \beta) \exp(-i2\pi f \beta) d\beta \right|^2 df \, dt$$

where I is the integration time of the photodetectors.

To summarize, if we assume that an integrating photodetector array is placed in the frequency plane, then a mathematical model that can be used to describe the signals produced by the AOSA and the one that will be used throughout this report is represented by the following equation

$$X_{jk} = \int_{jI}^{(j+1)I} \int_{-\infty}^{\infty} H(f - f_k) \left| \int_{-\infty}^{\infty} w(\beta)u(t - \beta)\exp(-i2\pi f\beta)d\beta \right|^2 df \, dt \qquad (1)$$

where X_{jk} is the voltage produced at the output of the kth detector for the jth integrated time frame. Basically, this equation implies that the instantaneous light intensity distribution shining on the array of photodetectors is the magnitude squared Fourier transform of the part of the signals that are contained in the Bragg cell at that time, windowed by the function $w(\beta)$. In addition, it implies that each photodetector in the frequency plane spatially integrates this light intensity distribution and converts it to currents which are integrated and sampled at periodic intervals of duration I.

In [7] we find a comparison between an extended version of this model and some experimental results, which serves to validate our model. It should be noted that the model that we will use in this report is often used [8][9] to perform analyses on the output signals of an AOSA.

When $u(t)$ is a pure sinusoid (which corresponds to the case where the input signal is a continuous-wave), the mathematical model represented by equation (1) can be rewritten in a more convenient form. To see this, we note that equation (1) can be rewritten as

$$X_{jk} = \int_{jI}^{(j+1)I} \int_{-\infty}^{\infty} \int_{-\infty}^{\infty} \int_{-\infty}^{\infty} H(f - f_k)w(\alpha)w^*(\beta)u(t - \alpha)u^*(t - \beta)$$
$$\exp\left[-i2\pi f(\alpha - \beta)\right] d\alpha \, d\beta \, df \, dt. \qquad (2)$$

If

$$u(t) = A\cos(2\pi f_0 t + \phi) \qquad (3)$$

then

$$u(t - \alpha)u^*(t - \beta) = A\cos\left[2\pi f_0(t - \alpha) + \phi\right] \cdot A\cos\left[2\pi f_0(t - \beta) + \phi\right] \qquad (4)$$
$$= \frac{A^2}{2}\left\{\cos\left[4\pi f_0 t - 2\pi f_0(\alpha + \beta) + 2\phi\right] + \cos\left[2\pi f_0(\alpha - \beta)\right]\right\}. \qquad (5)$$

Thus

$$X_{jk} = \frac{A^2}{2} \int_{jI}^{(j+1)I} \int_{-\infty}^{\infty} \int_{-\infty}^{\infty} \int_{-\infty}^{\infty} H(f - f_k)w(\alpha)w^*(\beta)\Big\{\cos\big[2\pi f_0(\alpha - \beta)\big]$$

$$+ \cos\big[4\pi f_0 t - 2\pi f_0(\alpha + \beta) + 2\phi\big]\Big\}\exp\big[-i2\pi f(\alpha - \beta)\big]\,d\alpha\,d\beta\,df\,dt \qquad (6)$$

$$= \frac{A^2}{2} \int_{-\infty}^{\infty} \int_{-\infty}^{\infty} \int_{-\infty}^{\infty} H(f - f_k)w(\alpha)w^*(\beta)\exp\big[-i2\pi f(\alpha - \beta)\big]$$

$$\int_{jI}^{(j+1)I} \Big\{\cos\big[2\pi f_0(\alpha - \beta)\big] + \cos\big[4\pi f_0 t - 2\pi f_0(\alpha + \beta) + 2\phi\big]\Big\}dt\,d\alpha\,d\beta\,df. \qquad (7)$$

In practical situations we can expect that $I \gg 1/4\pi f_0$ (the integration time of the system is over several periods of the CW signal) so that

$$\exp\big[-i2\pi f(\alpha - \beta)\big] \int_{jI}^{(j+1)I} \Big\{\cos\big[2\pi f_0(\alpha - \beta)\big] + \cos\big[4\pi f_0 t - 2\pi f_0(\alpha + \beta) + 2\phi\big]\Big\}dt$$

$$= \exp\big[-i2\pi f(\alpha - \beta)\big] \Big\{\cos\big[2\pi f_0(\alpha - \beta)\big]I$$

$$+ \Big[\frac{sin\big[4\pi f_0 t - 2\pi f_0(\alpha + \beta) + 2\phi\big]}{4\pi f_0}\Big|_{jI}^{(j+1)I}\Big\} \qquad (8)$$

$$\approx \exp\big[-i2\pi f(\alpha - \beta)\big]\cos\big[2\pi f_0(\alpha - \beta)\big]I \qquad (9)$$

$$= \frac{I}{2}\exp\big[-i2\pi f(\alpha - \beta)\big]\Big\{\exp\big[i2\pi f_0(\alpha - \beta)\big] + \exp\big[-i2\pi f_0(\alpha - \beta)\big]\Big\}$$

$$= \frac{I}{2}\Big\{\exp\big[-i2\pi(\alpha - \beta)(f - f_0)\big] + \exp\big[-i2\pi(\alpha - \beta)(f + f_0)\big]\Big\}. \qquad (10)$$

Substituting (10) in (7) we get that for $I \gg 1/4\pi f_0$

$$X_{jk} \approx \frac{A^2 I}{4} \int_{-\infty}^{\infty} \int_{-\infty}^{\infty} \int_{-\infty}^{\infty} H(f - f_k)w(\alpha)w^*(\beta)\Big\{\exp\big[-i2\pi(\alpha - \beta)(f - f_0)\big]$$

$$+ \exp\big[-i2\pi(\alpha - \beta)(f + f_0)\big]\Big\}d\alpha\,d\beta\,df. \qquad (11)$$

If we define

$$G(f) \triangleq \left|\int_{-\infty}^{\infty} w(t)\exp(-i2\pi ft)dt\right|^2 \qquad (12)$$

$$= \int_{-\infty}^{\infty} w(\alpha)\exp(-i2\pi f\alpha)d\alpha \int_{-\infty}^{\infty} w^*(\beta)\exp(i2\pi f\beta)d\beta$$

$$= \int_{-\infty}^{\infty} \int_{-\infty}^{\infty} w(\alpha)w^*(\beta)\exp\big[-i2\pi f(\alpha - \beta)\big]\,d\alpha\,d\beta \qquad (13)$$

then

$$G(f + f_0) = \int_{-\infty}^{\infty} \int_{-\infty}^{\infty} w(\alpha)w^*(\beta) \exp\left[-i2\pi(\alpha - \beta)(f + f_0)\right] d\alpha\, d\beta \qquad (14)$$

and similarly

$$G(f - f_0) = \int_{-\infty}^{\infty} \int_{-\infty}^{\infty} w(\alpha)w^*(\beta) \exp\left[-i2\pi(\alpha - \beta)(f - f_0)\right] d\alpha\, d\beta. \qquad (15)$$

Substituting (14) and (15) in (11) we get

$$X_{jk} \approx \frac{A^2 I}{4} \int_{-\infty}^{\infty} H(f - f_k) \left[G(f - f_0) + G(f + f_0)\right] df. \qquad (16)$$

Now if we assume that $H(f)$ is symmetrical about $f = 0$, then

$$\int_{-\infty}^{\infty} H(f - f_k)G(f + f_0)df = \int_{-\infty}^{\infty} H(f_k - f)G(f + f_0)df$$

$$= \int_{-\infty}^{\infty} H\left[f_k - (f + f_0) + f_0\right] G(f + f_0)df$$

$$= \int_{-\infty}^{\infty} H(f_k + f_0 - f')G(f')df' = \mathcal{H}(f_k + f_0), \qquad (17)$$

where

$$\mathcal{H}(f) = \int_{-\infty}^{\infty} H(f - f')G(f')df' \qquad (18)$$

which is the convolution between the functions $G(f)$ and $H(f)$. Clearly this is a function centered about the origin with bandwidth equal to the sum of the bandwidths of $G(f)$ and $H(f)$. If we note that

$$\mathcal{H}(f_k - f_0) = \int_{-\infty}^{\infty} H(f - f_k)G(f - f_0)df \qquad (19)$$

then by substituting (17) and (19) in (16) we get that

$$X_{jk} \approx \frac{A^2 I}{4} \left\{\mathcal{H}(f_k - f_0) + \mathcal{H}(f_k + f_0)\right\}. \qquad (20)$$

But since the passband of a practical Bragg cell for this application would normally be at frequencies which are high with respect to the bandwidth of $\mathcal{H}(f)$, then $\mathcal{H}(f_k + f_0)$ will be very small compared to $\mathcal{H}(f_k - f_0)$, and thus we have that for $I \gg 1/4\pi f_0$

$$X_{jk} \approx \frac{A^2 I}{4} \mathcal{H}(f_k - f_0). \qquad (21)$$

We shall adopt this mathematical model throughout this report and use

$$X_{jk} = \frac{A^2 I}{4} \mathcal{H}(f_k - f_0),\qquad(22)$$

where $\mathcal{H}(f)$ is the convolution between the functions $G(f)$ and $H(f)$,

$$\mathcal{H}(f) = \int_{-\infty}^{\infty} H(f - f')G(f')df'\qquad(23)$$

with $G(f)$ the magnitude squared of the Fourier transform of the window function

$$G(f) = \left| \int_{-\infty}^{\infty} w(t)\exp(-i2\pi ft)dt \right|^2.\qquad(24)$$

2.2.3 Numerical Calculations

When the input signal is a CW, $u(t) = A\cos(2\pi f_o t + \phi)$ and the output for the kth photodetector element X_{jk} can be obtained by appropriately sampling $\mathcal{H}(f)$ and multiplying by a scale factor, as can be seen from equation (22). In turn, samples of $\mathcal{H}(f)$ can be obtained by integrating portions of $G(f)$ as can be seen from equation (23). If $H(f)$ is a rectangular function, then samples of $\mathcal{H}(f)$ can be obtained by simply integrating $G(f)$ over the appropriate intervals and if not, then we need to window $G(f)$ according to $H(f)$ before we integrate.

In most of the cases of interest, there is no closed form solution to equation (23) and hence we must evaluate $\mathcal{H}(f)$ numerically. In fact, most of the time it is even difficult to obtain a closed form solution for $G(f)$ as defined in equation (24).

The derivations performed in the subsequent sections will be general and could be applied to any system configuration. However, for the numerical calculations in these sections we will always assume that $H(f)$ is a rectangular function of unit amplitude and width B Hz, symmetrical about $f = 0$. This is probably a reasonable assumption as it is unlikely that any practical $H(f)$ will affect our calculations to any great extent. In any case, the calculations could easily be redone for any $H(f)$.

In addition, the numerical calculations performed in the subsequent sections will only consider the case where $w(t)$ is a rectangular function of unit amplitude over the interval $[0, \tau]$. This truncation effect due to the finite size of the Bragg cell is certainly the most important factor to take into account. However, as it was mentioned in the previous subsection, there are other effects which may or may not need to be taken into account depending on the system configuration and the specific components that

are used in the system. The fact is that there could be many possibilities for $w(t)$, depending on the application.

Since there is such a large variation in $w(t)$, in this report we have chosen to do the numerical calculations only for the most basic case where $w(t)$ is a rectangular function. We assume that the reader interested in the calculations for another specific $w(t)$ will redo these calculations to see if they are very different from the calculations performed in this report. However, to give an appreciation of the effect of $w(t)$ on the signals produced by an AOSA, we will show how $G(f)$ can be calculated for some of the other specific cases of $w(t)$ and how this will affect the function $\mathcal{H}(f)$.

2.2.3.1 General case

A family of window functions $w(t)$ that is found to be useful [10] is given by

$$w(t) = \exp\left[-\alpha(f_0)t - 4T^2\left(\frac{t}{\tau} - \frac{1}{2}\right)^2\right] \text{rect}\left(\frac{t}{\tau} - \frac{1}{2}\right), \qquad (25)$$

where α (in nepers/sec) accounts for the acoustic amplitude attenuation and is a function of the input signal frequency, T accounts for the profile of practical laser beams and is the ratio of the truncated aperture over the e^{-2} intensity width of that Gaussian profile, and τ (in seconds) is the truncated aperture which is related to the physical length of the Bragg cell.

If $\alpha = 0$ (that is, if we assume that there are no propagation losses in the Bragg cell), we have that $w(t)$ is a truncated Gaussian profile. To see the effect of the acoustic attenuation on that window function, we can transform equation (25) into the following form

$$w(t) = \exp\left[-4T^2\left(\frac{t}{\tau} - \frac{1}{2} + \frac{\alpha\tau}{8T^2}\right)^2 + \frac{(\alpha\tau)^2}{16T^2} - \frac{\alpha\tau}{2}\right] \text{rect}\left(\frac{t}{\tau} - \frac{1}{2}\right) \qquad (26)$$

where we can see that the acoustic attenuation causes a shift in the peak position of the Gaussian profile as well as a decrease in the peak amplitude. However, the general shape of the window function is preserved.

In general, there is no closed form solution to the Fourier transform of equation (25). So unless some simplification or approximation is done, we cannot obtain a closed form expression for $G(f)$. Once we have obtained $G(f)$, we can easily obtain $\mathcal{H}(f)$ by numerically integrating $G(f)$ over finite periods since we assume that $H(f)$ is a rectangular weighting function.

We can estimate $G(f)$ numerically using the rectangular rule as

$$G(f) \approx G_a(f) \triangleq \left|\Delta t \sum_{m=0}^{M-1} w(m\Delta t)\exp(-i2\pi f m\Delta t)\right|^2. \qquad (27)$$

If we let $\Delta t = \tau/M$, where M is the number of points from $w(t)$ that will be used to calculate one sample of $G(f)$, then

$$G_a(f) = \left| \frac{\tau}{M} \sum_{m=o}^{M-1} w\left(\frac{m\tau}{M}\right) \exp\left(\frac{-i2\pi fm\tau}{M}\right) \right|^2 . \tag{28}$$

Defining $v = f\tau$, we get

$$G_a(v/\tau) = \left| \frac{\tau}{M} \sum_{m=0}^{M-1} w\left(\frac{m\tau}{M}\right) \exp\left(\frac{-i2\pi vm}{M}\right) \right|^2 \tag{29}$$

or if we express the complex component in rectangular coordinates, we get

$$G_a(v/\tau) = |\tau K(v)|^2 \tag{30}$$

where

$$K(v) = \frac{\sum_{m=0}^{M-1} \left[w\left(\frac{m\tau}{M}\right) \cos\left(\frac{2\pi vm}{M}\right) - iw\left(\frac{m\tau}{M}\right) \sin\left(\frac{2\pi vm}{M}\right) \right]}{M} \tag{31}$$

and hence

$$G_a(v/\tau) = \tau^2 \left\{ [Re(K)]^2 + [Im(K)]^2 \right\} . \tag{32}$$

To consider the error associated with the approximation of (32), let

$$X_a(f) = \Delta t \sum_{m=0}^{M-1} w(m\Delta t) \exp(-i2\pi fm\Delta t). \tag{33}$$

It is easy to see from (27) that

$$G_a(f) = |X_a(f)|^2. \tag{34}$$

We note that the Fourier transform of a delayed Dirac delta function $\delta(t - t_0)$ is $e^{-i2\pi ft_0}$. Thus we may regard (33) as the Fourier transform of $\Delta t \sum_{m=0}^{M-1} w(m\Delta t)\delta(t - m\Delta t)$, that is

$$X_a(f) = \mathcal{F}\left\{ \Delta t \sum_{m=0}^{M-1} w(m\Delta t)\delta(t - m\Delta t) \right\} . \tag{35}$$

Since $w(t)$ is zero outside the interval $[0, \tau]$, we may rewrite (35) as

$$X_a(f) = \mathcal{F}\left\{ w(t) \cdot \Delta t \sum_{m=-\infty}^{\infty} \delta(t - m\Delta t) \right\} \tag{36}$$

which can be transformed, using the well known property for the Fourier transform of multiplied time functions, to the following

$$X_a(f) = W(f) * \mathcal{F} \left\{ \Delta t \sum_{m=-\infty}^{\infty} \delta(t - m\Delta t) \right\},$$

which becomes

$$X_a(f) = W(f) * \sum_{m=-\infty}^{\infty} \delta\left(f - \frac{m}{\Delta t}\right)$$

which finally becomes

$$X_a(f) = \sum_{m=-\infty}^{\infty} W\left(f - \frac{m}{\Delta t}\right). \tag{37}$$

So we see that the approximation of equation (32) is in fact an aliased version of $G(f)$. We also see that $G_a(f)$ is periodic with period $1/\Delta t$, hence there is no point in calculating $G_a(f)$ outside the range of frequencies

$$\frac{-M}{2\tau} < f < \frac{M}{2\tau}$$

since $\Delta t = \tau/M$. Or if we use the normalized version $G_a(v/\tau)$, then the range of frequencies is

$$\frac{-M}{2} < v < \frac{M}{2}.$$

In summary, we have shown how the rectangular rule for numerical integration can be used to obtain an aliased version of $G(f)$. The resulting normalized numerical equation is

$$G_a(v/\tau) = \tau^2 \left\{ [Re\,(K(v))]^2 + [Im\,(K(v))]^2 \right\}, \tag{38}$$

where $v = f\tau$ and

$$K(v) = \frac{\sum_{m=0}^{M-1} \left[w\left(\frac{m\tau}{M}\right) \cos\left(\frac{2\pi v m}{M}\right) - i w\left(\frac{m\tau}{M}\right) \sin\left(\frac{2\pi v m}{M}\right) \right]}{M}, \tag{39}$$

where M is the number of sample points from $w(t)$ that will be used to calculate one sample of $G(f)$. We see that the above algorithm is closely related to the DFT algorithm except for the fact that it can be used to obtain samples of $G(f)$ at any

frequency instead of obtaining those for a fixed set of frequencies. Normalizing $w(t)$ to the following equation

$$w(x\tau) = \exp\left[-Lx - 4T^2\left(x - \frac{1}{2}\right)^2\right] \text{rect}\left(x - \frac{1}{2}\right), \qquad (40)$$

where $L = \alpha\tau$ and $x = t/\tau$, makes it easy to calculate equation (38). $G_a(v/\tau)$ is periodic with a period of M with respect to v, so it should only be used to calculate samples of $G(v/\tau)$ for the range $\frac{-M}{2} < v < \frac{M}{2}$. Since $G_a(f)$ is an aliased version of $G(f)$, M should be made large enough to make this error insignificant and we should not attempt to calculate samples of $G(f)$ which are lower than a certain value. The value of M and the lowest value of $G(f)$ that we attempt to calculate using $G_a(v/\tau)$ depend on $G(f)$, so determining this may require some trial and error. When $\alpha = 0$ and $T = 0$, $w(t)$ is simply a rectangular window and $G(f)$ is a squared Sinc function. For that case, the sidelobe level is down approximately 50 dB from the peak at a frequency of $100/\tau$. For all other cases, the sidelobes will decrease even more rapidly.

Figure 2 shows the window function $w(t)$ for the case of $\alpha\tau = 0.5$, $T = 1$. Figure 3 shows the function $G(f)$ calculated from equation (38) using $M = 200$ for the same case of $\alpha\tau = 0.5$, $T = 1$. Finally, Figure 4 shows $\mathcal{H}(f)$ for that same case assuming the photodetectors have a bandwidth of $B = 1/\tau$. It should be noted that $\mathcal{H}(f)$ is symmetrical about $f = 0$ even though this is not shown on Figure 4. This last figure is the result of numerically integrating the function $G(f)$. For that reason it is useful to have a numerical algorithm that can calculate samples of $G(f)$ at any frequency because most numerical integration programs require a function which can do that.

2.2.3.2 Untruncated Gaussian windowing

We have showed how the output of the AOSA could be calculated using an algorithm which has calculations similar to those encountered in the direct evaluation of the DFT. But it has long been recognized that the DFT is computationally expensive. In fact it is presumed that Carl Friedrich Gauss, the eminent German mathematician, developed an algorithm that could simplify its calculation as early as the year 1805 [11].

It is therefore worthwhile to note that if we assume $\alpha = 0$ and the Gaussian shaping is not truncated by the physical size of the Bragg cell, then we can get a closed form expression for $G(f)$. Harms and Hummels have used this result in [9] and have calculated the transform of $w(t)$ by means of a line integral in the complex plane.

In this case we have that

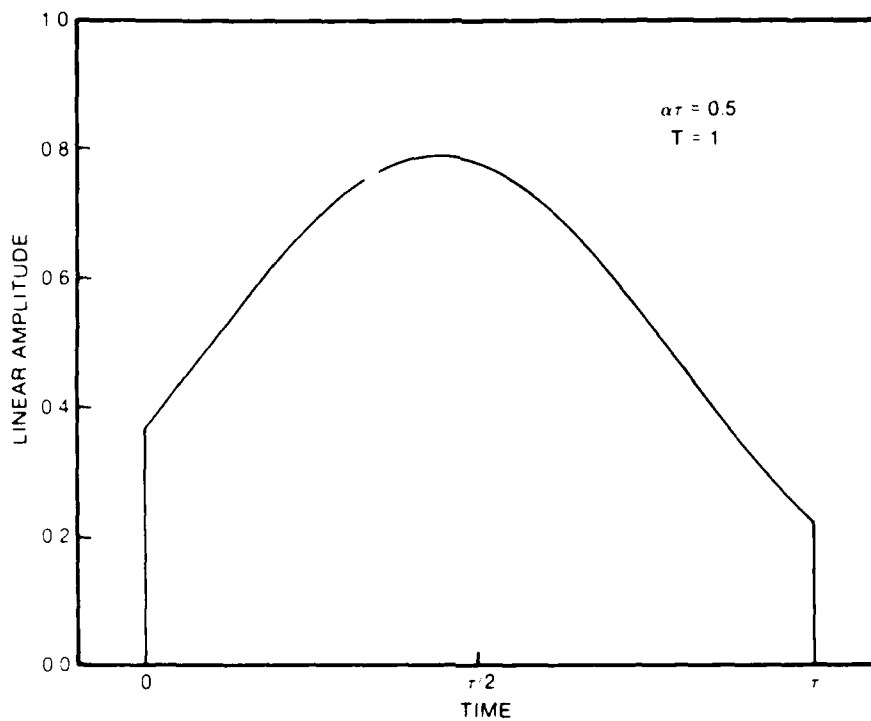$$w(t) = \exp\left[-4T^2\left(\frac{t}{\tau} - \frac{1}{2}\right)^2\right] \qquad (41)$$

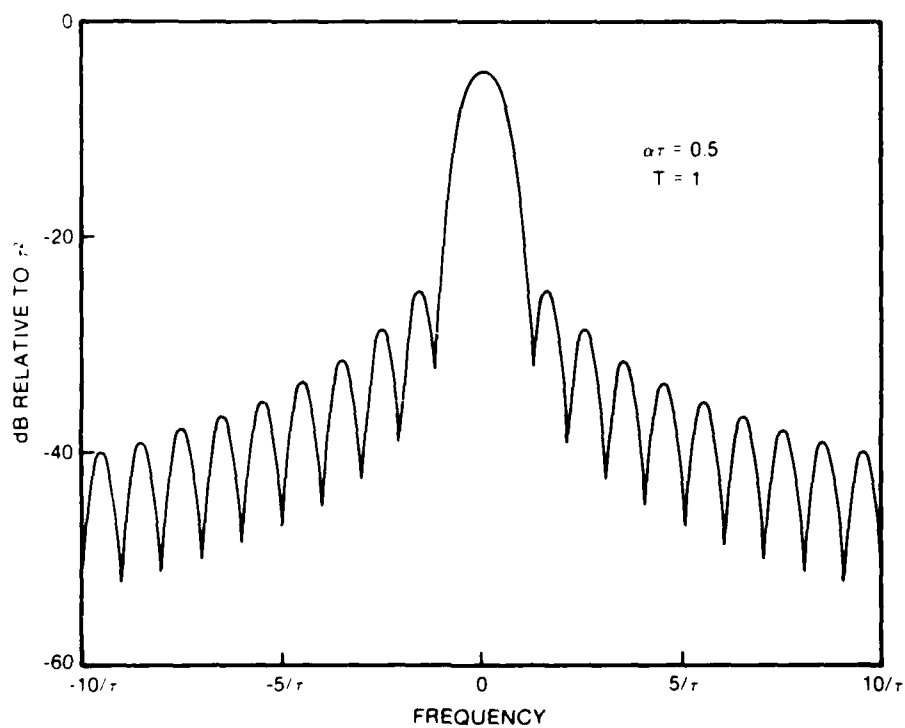FIGURE 2:   WINDOW $w(t)$ WHEN $\alpha\tau = 0.5, T = 1$

FIGURE 3: $G(f)$ WHEN $\alpha\tau = 0.5, T = 1$

FIGURE 4: $\mathcal{H}(f)$ FOR $\alpha\tau = 0.5, T = 1, \tau B = 1$

so that

$$G(v/\tau) = \tau^2 \frac{\pi}{4T^2} \exp\left(\frac{-\pi^2 v^2}{2T^2}\right) \tag{42}$$

where again $v = f\tau$. This greatly simplifies the calculation of $\mathcal{H}(f)$ but it should only be used when T is large. (In [9] this approximation for $T = 1.63$ is used and it is claimed that the resultant error is negligible.)

Figure 5 shows the window function, $w(t)$ for the case of $T = 2$ while Figure 6 shows the function $G(f)$ calculated using equation (42). Finally, Figure 7 shows $\mathcal{H}(f)$ for that same case assuming the photodetectors have a bandwidth of $B = 1/\tau$.

2.2.3.3 Truncated exponential windowing

If we assume that $T = 0$, that is if we assume that the laser has no Gaussian shaping but we still want to take into account the fact that there is attenuation of the acoustic wave as it propagates through the Bragg cell, then $w(t)$ is given by

$$w(t) = \exp(-\alpha t)\operatorname{rect}\left(\frac{t}{\tau} - \frac{1}{2}\right) \tag{43}$$

FIGURE 5: WINDOW $w(t)$ WHEN $\alpha\tau = 0$, $T = 2$
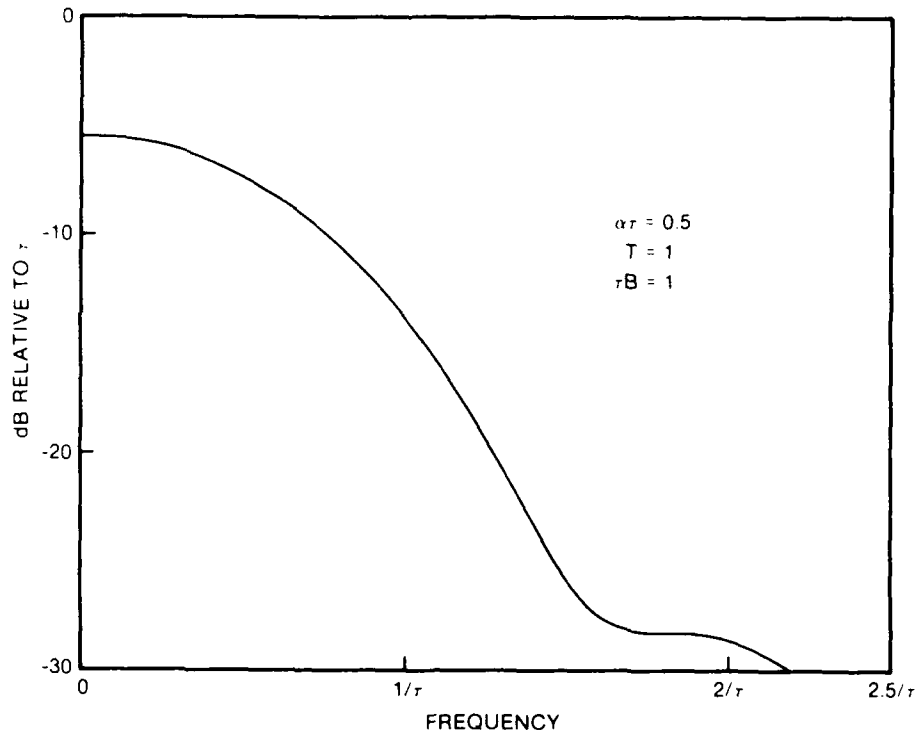

FIGURE 6: $G(f)$ WHEN $\alpha\tau = 0$, $T = 2$

FIGURE 7: $\mathcal{H}(f)$ FOR $\alpha\tau = 0$, $T = 2$, $\tau B = 1$

and so

$$G(v/\tau) = \tau^2 \frac{\left[1 - 2e^{-L}\cos(2\pi v) + e^{-2L}\right]}{L^2 + (2\pi v)^2}.$$ (44)

Figure 8 shows the window function $w(t)$ for the case of $\alpha\tau = 0.5$ while Figure 9 shows the function $G(f)$ calculated using equation (44). Finally, Figure 10 shows $\mathcal{H}(f)$ for that same case assuming the photodetectors have a bandwidth of $B = 1/\tau$.

2.2.3.4 Rectangular windowing

As it was mentioned earlier, if we ignore the acoustic loss of the Bragg cell and the Gaussian shaping of the laser, then $w(t)$ is simply a rectangular window whose duration is determined by the physical size of the crystal or the width of the light wave impinging on the cell. For that case it is easy to show that $w(t)$ is as shown in Figure 11 and $G(f)$ is given by the following equation

$$G(f) = \tau^2 \frac{\sin^2(2\pi f\tau/2)}{(2\pi f\tau/2)^2}$$ (45)

which is shown in Figure 12. The resulting function $\mathcal{H}(f)$ for $\tau B = 1$ is shown in Figure 13.

FIGURE 8: WINDOW $w(t)$ WHEN $\alpha\tau = 0.5$, $T = 0$

FIGURE 9: $G(f)$ WHEN $\alpha\tau = 0.5$, $T = 0$

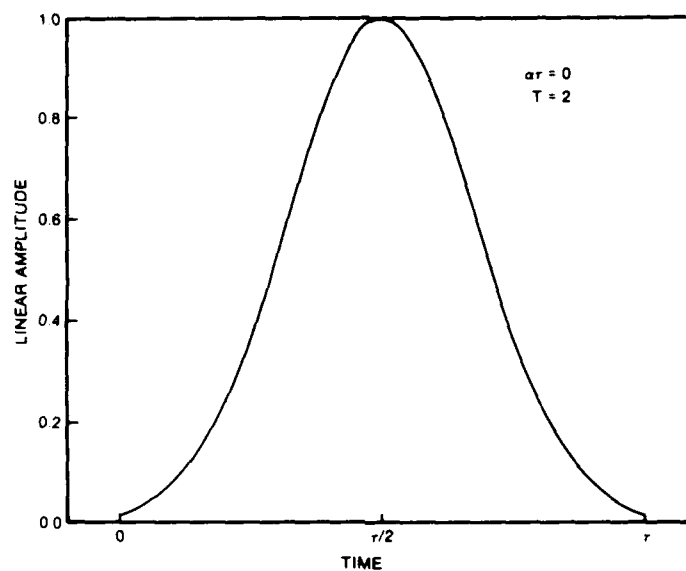FIGURE 10: $\mathcal{H}(f)$ FOR $\alpha\tau = 0.5$, $T = 0$, $\tau B = 1$

FIGURE 11: WINDOW $w(t)$ WHEN $\alpha\tau = 0$, $T = 0$
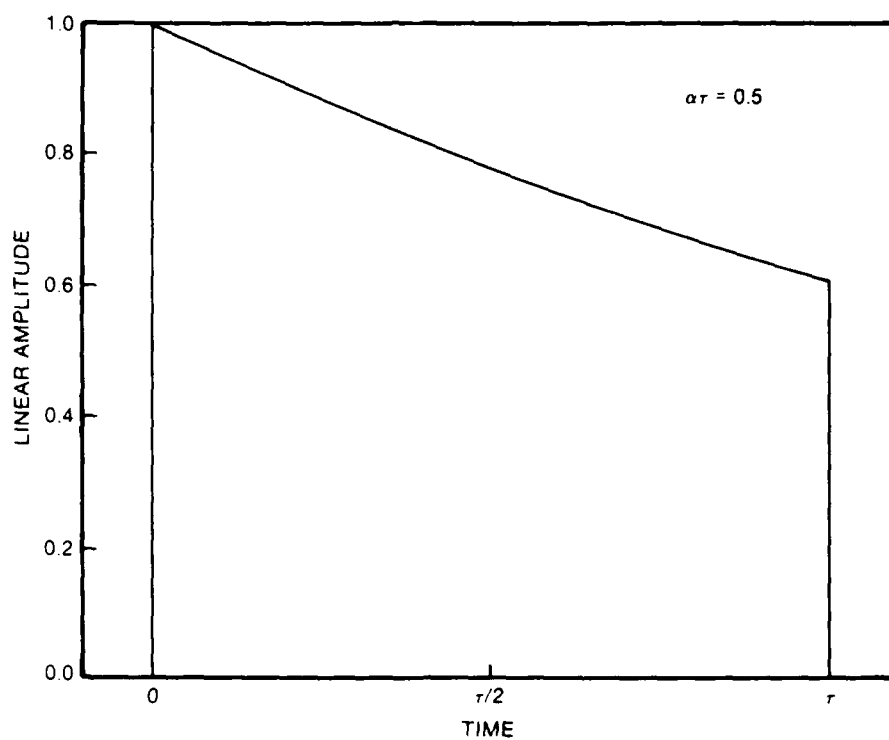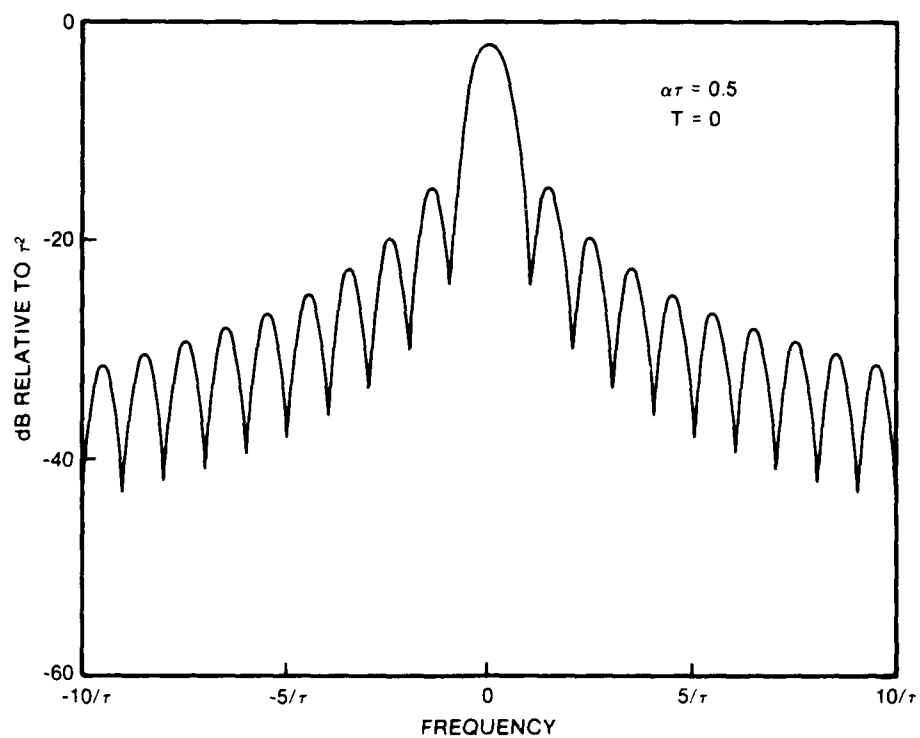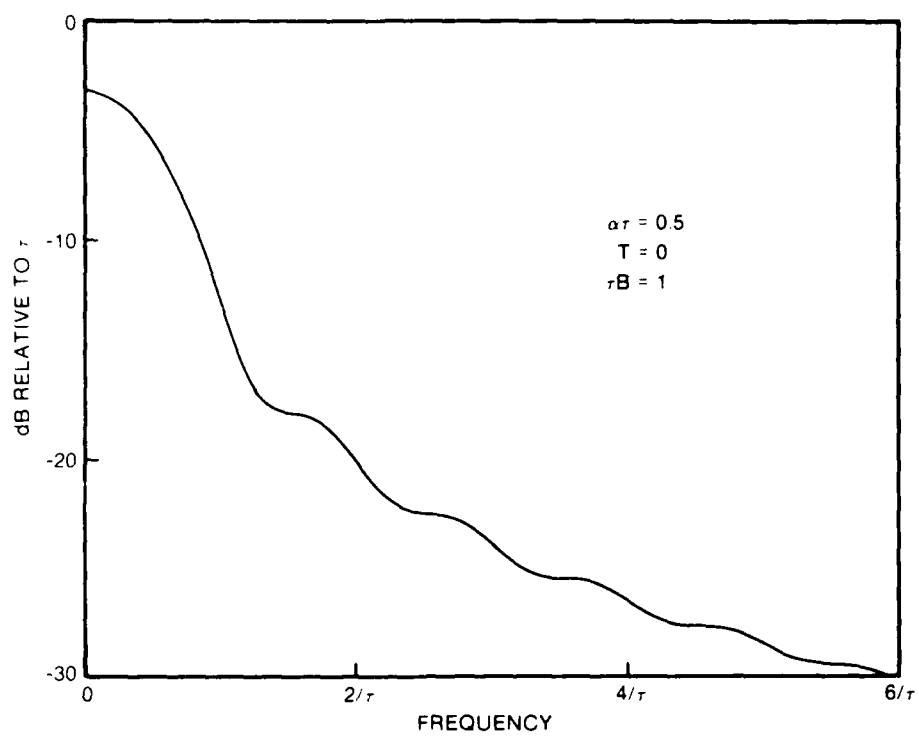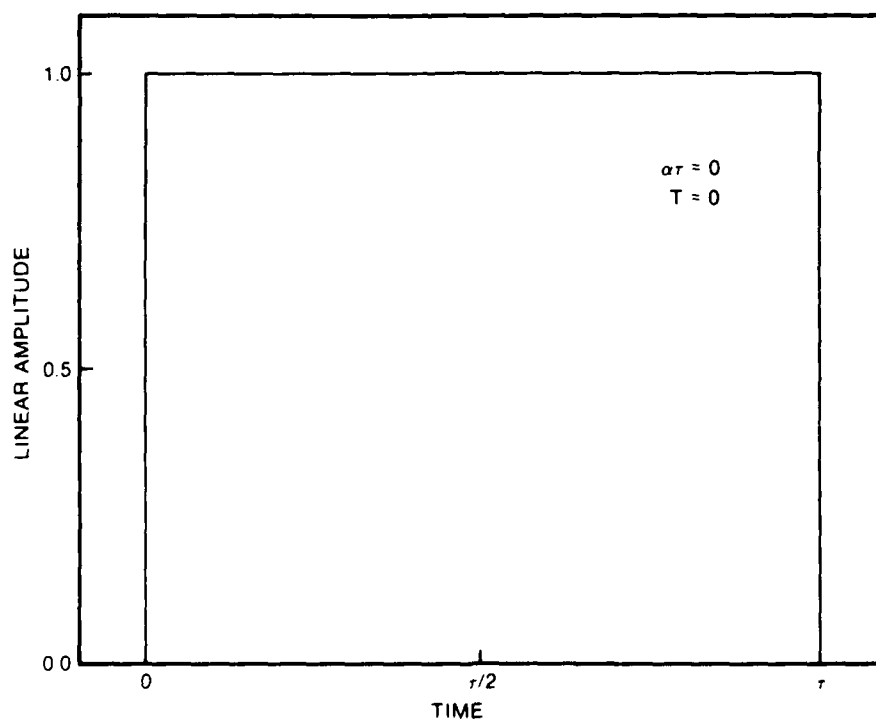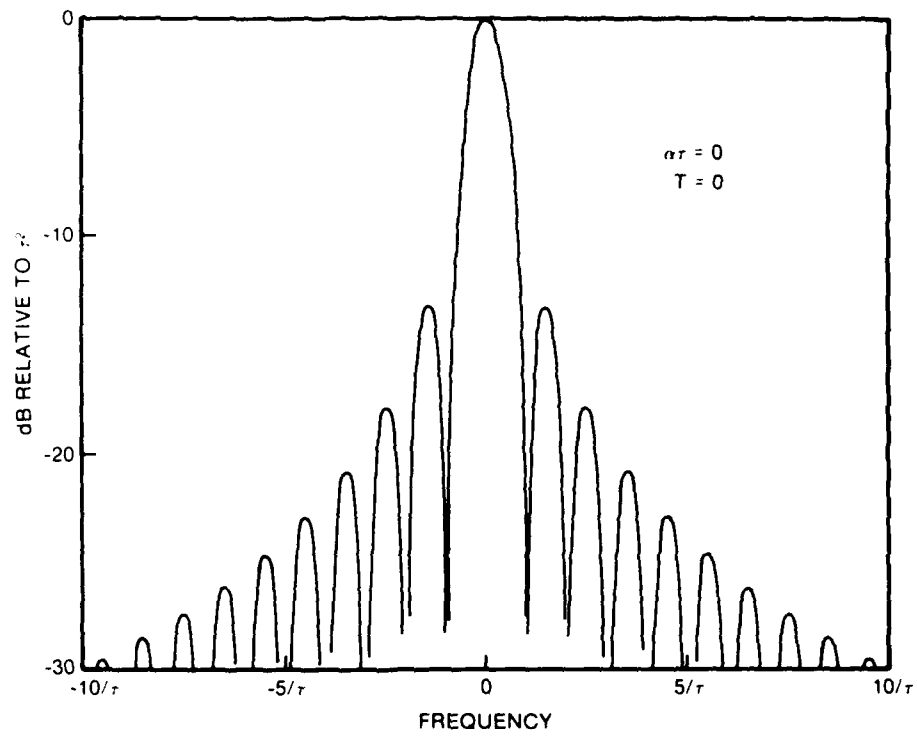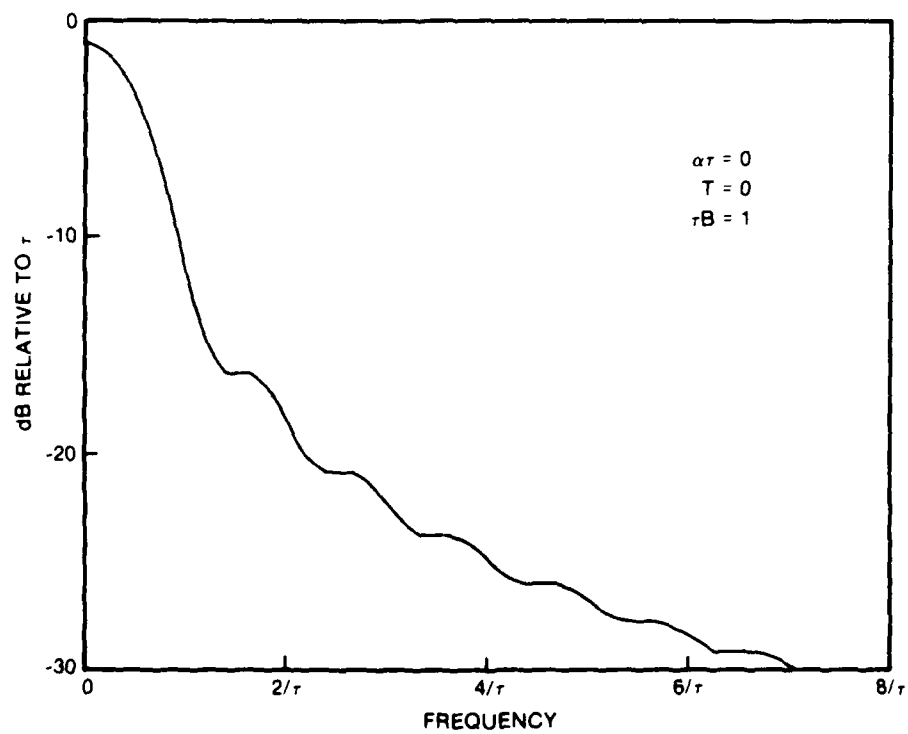
FIGURE 12: $G(f)$ WHEN $\alpha\tau = 0, T = 0$

FIGURE 13: $\mathcal{H}(f)$ FOR $\alpha\tau = 0, T = 0, \tau B = 1$

2.3 Noise Model

In the previous subsection, we presented the AOSA configuration of interest in this report along with a mathematical model to calculate the deterministic component of the photodetector output. In addition to the deterministic component due to the input signal, the photodetector output is corrupted by noise from a variety of sources. Among the possible noise contributors we can include the laser, the microwave front-end, the photodetectors, vibration and scattered light.

In the application that we are considering, we are always striving to design receivers with high dynamic range and good sensitivity. When designing an AOSA for this application, we usually find that the photodetectors are the bottleneck in terms of those requirements. This means that the photodetector noise is dominant among the other sources of noise.

In [12] we performed experimental measurements on the noise of an avalanche photodiode (APD) array. This array is of special interest for the design of systems to monitor the electromagnetic environment because of its high sensitivity. The measurements were done using an analog amplifier which would typically be used for this application. It was found that the distributions governing the noise present in the photodetector element outputs were Gaussian or normal distributions. The means of the probability density functions were found to vary significantly from element to element although their variances were roughly the same.

In light of these findings, we will assume in this report that the signal components of the detector elements are corrupted by additive Gaussian random variables independent of each other but having identical variances. In addition, we will assume that these random variables have zero means since in practice these noise offsets would most likely be subtracted out. Hence, the noise model that will be used in this report is that each photodetector output will be corrupted by independent, identically-distributed zero-mean Gaussian variables with variance σ^2.

2.4 Signal Plus Noise Model

Having presented the signal model and the noise model that will be used in this report, we will now present the complete signal plus noise model which will be used in the subsequent statistical analyses. To this end, let us first define

$$\bar{R} = \{r_1, r_2, r_3, \ldots, r_N\} \tag{46}$$

as the received vector which is used to represent the photodetector outputs after any integration time frame. We will sometimes refer to the photodetector outputs as the *pixel* outputs since this is an expression which is often used in this field.

We note that $\bar{R}$ is a vector in an N-dimensional space where N is the number of photodetector elements used in the linear array. We also note that

$$r_i = m_i(f_o, A) + n_i, \qquad i = 1, 2, 3, \ldots, N \tag{47}$$

were the n_i's are zero-mean, independent identically-distributed random variables with variance σ^2. It is important to realize that $m_k = X_{jk}$ in equation (1). We have chosen to henceforth use the later notation (i.e. m_i) to reflect the fact that the signal components of the r_i's are actually the *means* of these random variables. It is equally important to note that the m_i's are completely defined once we know the frequency f_o and the amplitude A of the input signal.

In the following sections, we will use this signal plus noise model and proceed to perform statistical analyses in an effort to obtain efficient post-processing algorithms. We will look at the detection as well as the frequency and power estimation problems.

3.0 DETECTION

3.1 Introduction

The first problem that we face when processing the output signals of an AOSA is the detection problem. That is, we must first make a decision as to whether one or more signals are present before we try to estimate their respective frequency and power.

In order to find an optimal solution for this problem, we must first define a criteria upon which this optimality is to be decided. One criterion that is commonly used in classical detection theory is the Bayes' criterion. The use of this criterion requires the existence of a priori statistics of the observed signal. This criterion cannot be used in the present circumstance since no meaningful a priori statistics can be assigned. The standard method of dealing with such situations is to use the Neyman-Pearson criterion.

The Neyman-Pearson criterion considers the conditional probability of deciding that a signal is present given that there is in reality no signal present (the *false alarm probability* P_F) and the conditional probability of deciding that a signal is present given that there is indeed a signal present (the *probability of detection* P_D). In applying the Neyman-Pearson criteria, we like to design a test which minimizes P_F and maintains P_D as large as possible. These turn out to be two conflicting objectives and so a tradeoff must be made. A specific aim in applying the Neyman-Pearson criterion is to maximize P_D while maintaining P_F less than a specified amount ξ, that is maximize P_D subject to $P_F \leq \xi$. This is the criterion that we will use in the remaining subsections of this section in dealing with the detection problem we face.

The first thing to note about this detection problem is that we are dealing with a composite hypothesis situation. This is because we seek to detect the presence of a

signal of which we do not know the frequency or the amplitude. We sometimes refer to these unknown parameters of a composite hypothesis problem as *unwanted* parameters since we do not care about them for the purposes of detection; we simply want to decide whether one or more signals are present irrespective of these parameters.

In the next subsection, we simply assume that these parameters (the frequency and the amplitude) are known and we go about deriving the optimum test and its performance. This is a logical thing to do because in certain instances, by assuming the *unwanted* parameters are known, we obtain a test which turns out to be independent of these parameters. We refer to such a test as a *uniformly most powerful* (UMP) test. It turns out, as we will show in the next subsection, that the optimum test we obtain is in fact independent of the amplitude of the input signal. However, it is dependent on its frequency. In the third subsection, we deal with this by using the test obtained in section 3.2 to decide on the presence of a number of possible frequencies within the bandwidth of our receiver. We obtain a scheme which has a good performance and which is easily implemented.

3.2 Detection of a Known Frequency

In this subsection we will find the optimum detection test under the Neyman-Pearson criterion for the situation where we want to decide whether a CW signal with a given frequency is present or not. To this end, we let

$$\bar{R} = \{r_1, r_2, r_3, \ldots, r_N\}$$

be the received vector where the r_i's are the pixel output values for a given frame. We can consider this problem as a binary hypothesis test where H_0 is the hypothesis that no signal is present and H_1 is the hypothesis that a signal is present and hence we can write

$$
\begin{aligned}
H_0 &: r_i = n_i, \\
H_1 &: r_i = m_i(f_0, A) + n_i, \qquad i = 1, 2, 3, \ldots, N
\end{aligned}
\tag{48}
$$

where the n_i's are zero-mean, independent identically-distributed Gaussian random variables with variance σ^2, the m_i's are the signal components, N is the number of pixels in the photodetector array and f_0, A are respectively the frequency and amplitude of the input signal as defined in equation (3). Referring to equation (1), we have that $m_k = X_{jk}$, but we will henceforth use this latter notation to denote the fact that the signal components are the means of the Gaussian random variables at the output of the AOSA. From (22) we have that

$$m_i = \frac{A^2 I}{4} \mathcal{H}_i \tag{49}$$

where it is understood that the $\mathcal{H}_i$'s are the samples of $\mathcal{H}(f)$ corresponding to the frequency and pixel under consideration (i.e. $\mathcal{H}_i = \mathcal{H}(f_i - f_0)$).

It is well known [13, pp. 34] that the optimum test according to the Neyman-Pearson criterion is satisfied by the likelihood ratio test

$$\Lambda(\bar{R}) \underset{H_0}{\overset{H_1}{\gtrless}} \lambda \tag{50}$$

where the likelihood ratio test is defined as

$$\Lambda(\bar{R}) \triangleq \frac{p(\bar{R} \mid H_1)}{p(\bar{R} \mid H_0)} \tag{51}$$

where $p(\bar{R} \mid H_i)$ is the conditional probability density function of the received vector $\bar{R}$ given that hypothesis H_i is true and λ is some threshold depending on the constraint $P_F \leq \xi$. This latter quantity can be determined from noting that

$$P_F = \int_\lambda^\infty p(\Lambda(\bar{R}) \mid H_0) d\Lambda(\bar{R}). \tag{52}$$

It is easy to show that for our problem as it is defined in (48), the above conditional probabilities are as follows

$$p(\bar{R} \mid H_0) = \prod_{i=1}^N \frac{1}{\sqrt{2\pi\sigma^2}} \exp\left(\frac{-r_i^2}{2\sigma^2}\right) \tag{53}$$

$$p(\bar{R} \mid H_1) = \prod_{i=1}^N \frac{1}{\sqrt{2\pi\sigma^2}} \exp\left[\frac{-(r_i - m_i)^2}{2\sigma^2}\right] \tag{54}$$

and hence the likelihood function can be written as

$$\Lambda(\bar{R}) = \exp\left(\frac{\sum_{i=1}^N r_i^2 - \sum_{i=1}^N (r_i - m_i)^2}{2\sigma^2}\right) \tag{55}$$

$$= \exp\left(\frac{2\sum_{i=1}^N r_i m_i - \sum_{i=1}^N m_i^2}{2\sigma^2}\right). \tag{56}$$

But because the natural logarithm is a monotonic function and both sides of equation (50) must be positive, the likehood ratio test is equivalent to the test

$$\ln\{\Lambda(\bar{R})\} \underset{H_0}{\overset{H_1}{\gtrless}} \ln(\lambda) \tag{57}$$

which is very useful given the form of $\Lambda(\bar{R})$ as shown in equation (56).

Indeed, we can say that a test satisfying the Neyman-Pearson criterion for our problem is as follows

$$\frac{2\sum_{i=1}^{N} r_i m_i - \sum_{i=1}^{N} m_i^2}{2\sigma^2} \underset{H_0}{\overset{H_1}{\underset{<}{\gtrless}}} \ln(\lambda). \qquad (58)$$

This is equivalent to the test

$$\sum_{i=1}^{N} r_i m_i \underset{H_0}{\overset{H_1}{\underset{<}{\gtrless}}} \gamma, \qquad (59)$$

where γ is some constant.

It should be noted that hypothesis H_1 is a composite hypothesis because it contains the *unwanted* parameter A and the test of equation (59) cannot be used unless we know the value of A. However, since

$$m_i = \frac{A^2 I}{4}\mathcal{H}_i$$

we can reduce the above test to the following

$$\sum_{i=1}^{N} r_i \mathcal{H}_i \underset{H_0}{\overset{H_1}{\underset{<}{\gtrless}}} \gamma' \qquad (60)$$

because $A^2 I$ is a positive quantity. If we let

$$Y = \sum_{i=1}^{N} r_i \mathcal{H}_i$$

then the above test becomes

$$Y \underset{H_0}{\overset{H_1}{\underset{<}{\gtrless}}} \gamma' \qquad (61)$$

and

$$P_F = \int_{\gamma'}^{\infty} p(Y \mid H_0) dy. \qquad (62)$$

The above test is what is called a *uniformly most powerful* (UMP) test because it is completely defined (including threshold) for a given P_F without knowledge of the parameter A, which is the amplitude of the input signal. Of course, the performance of this test will be a function of this parameter as will be shown shortly.

In order to find the performance of this test, we note that if H_0 is true then Y is a Gaussian random variable with zero mean and variance

$$\sigma_Y^2 = \sigma^2 \sum_{i=1}^{N} \mathcal{H}_i^2.$$

And similarly, if H_1 is true then Y is a Gaussian random variable with mean

$$\bar{Y} = \sum_{i=1}^{N} m_i \mathcal{H}_i = \frac{A^2 I}{4} \sum_{i=1}^{N} \mathcal{H}_i^2$$

and variance

$$\sigma_Y^2 = \sigma^2 \sum_{i=1}^{N} \mathcal{H}_i^2.$$

From this we have that

$$P_F = \int_{\gamma'}^{\infty} \frac{1}{\sigma_Y \sqrt{2\pi}} \exp\left(\frac{-x^2}{2\sigma_Y^2}\right) dx \qquad (63)$$

or

$$P_F = \frac{1}{2} \operatorname{erfc}\left(\frac{\gamma'}{\sqrt{2}\sigma_Y}\right) \qquad (64)$$

where

$$\operatorname{erfc}(t) = \frac{2}{\sqrt{\pi}} \int_{t}^{\infty} \exp(-t^2) dt \qquad (65)$$

and

$$P_D = \int_{\gamma'}^{\infty} \frac{1}{\sqrt{2\pi}\sigma_Y} \exp\left[\frac{-(x - \bar{Y})^2}{2\sigma_Y^2}\right] dx \qquad (66)$$

or

$$P_D = \frac{1}{2} \operatorname{erfc}\left(\frac{\gamma' - \bar{Y}}{\sqrt{2}\sigma_Y}\right). \qquad (67)$$

Figure 14 shows the performance of the test of equation (60) as a function of the parameter

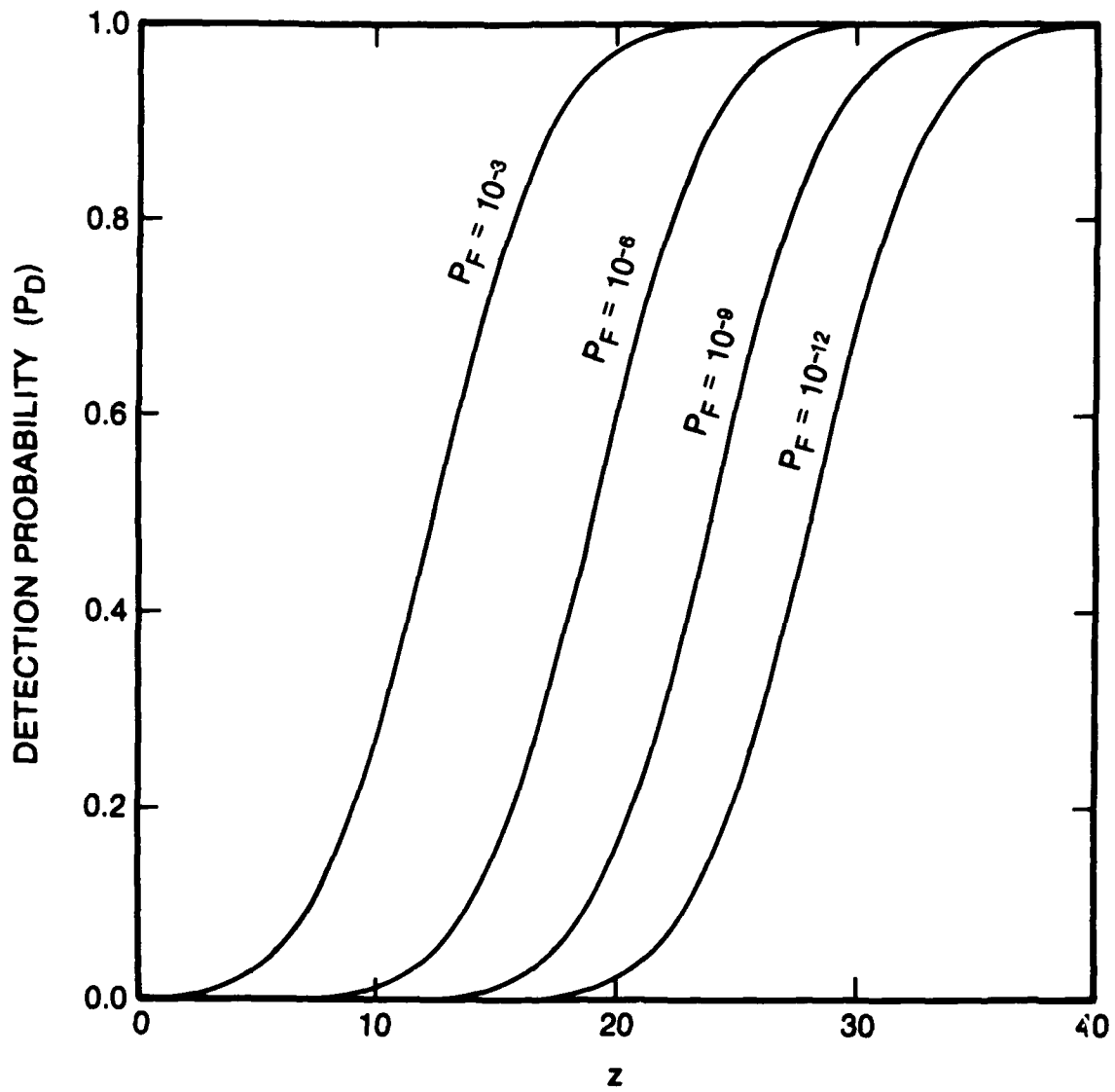$$z = \frac{A^2 I}{\sigma} \sqrt{\sum_{i=1}^{N} \mathcal{H}_i^2} \qquad (68)$$

FIGURE 14:   PERFORMANCE OF THE MATCHED FILTER

which serves as a figure of merit. Indeed z is the S/N ratio times the integration time of the photodetectors (I) times a factor which quantifies the performance gain due to the matched filter. We can see that the performance gain due to the matched filter depends on the number of pixels that are used in the algorithm. In Appendix I we calculate $\sum_{i=1}^{N} \mathcal{H}_i^2$ for different values of the constant τB. Of course, in practice we would not use N values of the $\mathcal{H}_i$'s in equation (60) to implement this test because some of these values will be insignificantly small. Using Figure 14 and equation (68) we could find a reasonable number of $\mathcal{H}_i$'s to use in our test for a given system configuration.

3.3   Detection of an Unknown Frequency

In the previous subsection, we looked at the optimum detection test using the Neyman-Pearson criterion for the case of a signal with known frequency. We have found that the optimum test for that case is the matched filter and we have also characterized its performance. However, for our application which is to use an AOSA to monitor the electromagnetic environment, we are not only interested in testing for the presence of one known frequency, but rather we are interested in testing for the presence of a range of unknown frequencies.

We can approach this problem by dividing the bandwidth of our receiver into a set of possible frequencies such that the resultant sequence forms a fine mesh over the whole bandwidth. Having done this, we can then use the matched filter to sequentially test for the presence of each one of these possible frequencies. We know that this test will be optimum if the input signal frequency corresponds to one of the possible frequencies that we have selected for our set.

A natural and convenient spacing for this set of possible frequencies is B, the frequency width of each photodetector. The reason for this is that, once we have selected the length of the matched filter, let us say n pixels, then we can simply slide the matched filter over the whole array, comparing its output against a threshold. This is simply a Finite Impulse Response (FIR) filter algorithm and is easily implemented as photodetector arrays often use serial output structures.

The advantage of this scheme is that we need not change the threshold value that we have selected according to the false alarm probability that we are willing to live with. Of course, something different will have to be done for the frequencies near the edge of the array. We could simply not consider the edge frequencies if the value of n is small or we could change the value of the threshold for these edge frequencies. When a strong signal is present, the output of the FIR filter will likely exceed the threshold for more than one frequency, but this is acceptable since we are using this scheme to detect the presence of signals and not to estimate the frequencies of those signals.

This scheme will optimally detect the presence of all the frequencies selected in our set of possible frequencies under the constraint of a given false alarm probability. We might want to know how this detection scheme performs for the frequencies that

are not included in this set; we cannot, after all expect to have a frequency line up with a photodetector center frequency. To answer this question, let us consider the more general case of how the performance of the test of equation (60) is affected when the $\mathcal{H}_i$'s used in the test are different from the $\mathcal{H}_i$'s that correspond to the signal. This could happen when the frequency of the input signal is different from the one we assumed with the $\mathcal{H}_i$'s of the filter or when the window function $w(t)$ that we used to calculate the $\mathcal{H}_i$'s was not accurately measured or for any other reason.

To calculate this effect on performance let

$$\tilde{Y} = \sum_{i=1}^{N} r_i \tilde{\mathcal{H}}_i \quad \mathop{\gtrless}_{H_0}^{H_1} \quad \gamma' \tag{69}$$

be the test, where the $\tilde{\mathcal{H}}_i$'s are used in the test but do not actually correspond to the $\mathcal{H}_i$'s of the signal. In this case, if H_0 is true, $\tilde{Y}$ is a Gaussian random variable with zero mean and variance

$$\sigma_{\tilde{Y}}^2 = \sigma^2 \sum_{i=1}^{N} \tilde{\mathcal{H}}_i^2.$$

But if H_1 is true, then $\tilde{Y}$ is a random variable with mean

$$E\{\tilde{Y}\} = \sum_{i=1}^{N} \tilde{\mathcal{H}}_i m_i = \frac{A^2 I}{4} \sum_{i=1}^{N} \tilde{\mathcal{H}}_i \mathcal{H}_i$$

and variance

$$\sigma_{\tilde{Y}}^2 = \sigma^2 \sum_{i=1}^{N} \tilde{\mathcal{H}}_i^2.$$

It is easy to show that the performance of the test of equation (69) is the same as the performance of the UMP test as shown in Figure 14 except that for this case

$$z = \frac{A^2 I \sum_{i=1}^{N} \tilde{\mathcal{H}}_i \mathcal{H}_i}{\sigma \sqrt{\sum_{i=1}^{N} \tilde{\mathcal{H}}_i^2}}. \tag{70}$$

We can therefore take the ratio of equation (70) and (68) to find the degradation in detection performance when the input signal frequency is *between* two pixels but the matched filter used is designed to test for the case when the input signal frequency *corresponds* to one pixel. Figure 15 shows this degradation for different values of the constant τB assuming rectangular windowing. We have used a matched filter with

25 taps to calculate the curves of Figure 15 and this assures us that all the $\mathcal{H}_i$'s that were dropped were insignificantly small. In Figure 15, we have only calculated the degradation over one period since the degradation is periodic with period B. As an illustration of how to interpret Figure 15, a degradation of 1 dB means that the input signal power would have to be 1 dB higher to obtain the same probability of detection as if the input signal frequency corresponded to the frequency of a pixel, everything else being the same.

We can see from this figure that for a given τB, the worst case degradation of the matched filter occurs when the input signal frequency is exactly in the middle of two f_k's. We also see that this worst case degradation increases for larger values of τB. However, we should note that even for $\tau B = 3$ the worst case degradation is less than 1.5 dB, a relatively small figure. Another important fact to note about Figure 15 is that most of the degradation is concentrated in a relatively small frequency range. This can be seen by the steepness of the curves at the point where the input signal frequency is exactly in the middle of two f_k's.

Hence we can see that the sliding matched filter scheme has a very good performance for the detection of unknown frequencies. The worst case degradation is relatively small and most of the degradation occurs over a relatively small frequency range.
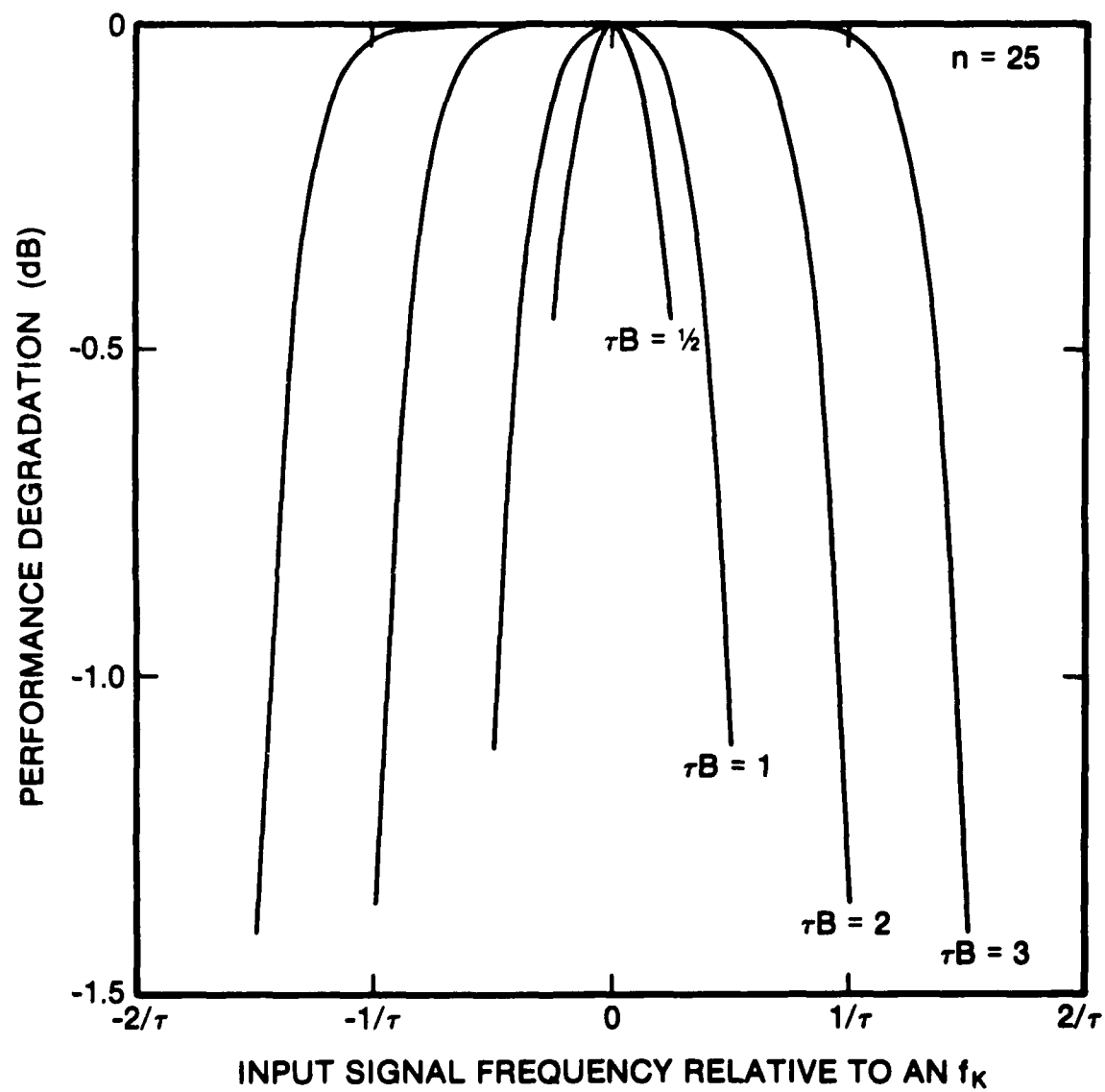
FIGURE 15: PERFORMANCE DEGRADATION OF THE MATCHED FILTER

4.0 ESTIMATION OF THE FREQUENCY

4.1 Introduction

The most important function of the AOSA receiver is to determine the frequency of the input signals. In this section, we will consider the problem of processing the output signals of the AOSA for the purpose of estimating the input signal frequency. We will approach this problem using classical estimation theory as expounded by Van Trees [13].

Classical estimation theory is divided into two main branches: the first is random parameters estimation and the second is nonrandom parameters estimation. Random parameters estimation requires some knowledge of the a priori probabilities for the outcome of the values of the parameters that we wish to estimate. In many cases, and certainly in the case of a receiving system that monitors the electromagnetic environment, it is unrealistic to treat the unknown parameter as a random variable. When dealing with a nonrandom parameter situation, we must work with the a posteriori density functions and evaluate the performance of different estimators by considering their bias and variance.

A useful landmark for the nonrandom parameter situation is the Cramér-Rao bound which gives us the lower bound on the variance of any unbiased estimator. In the next subsection, we present this bound and show its dependence on basic system design parameters. We shall see that this bound is useful since it shows us that, for this problem, any practical estimator of any significance would have to be biased. Hence in the third subsection of this section we present the performance of a practical estimator, the peak-detecting estimator. This estimator is a biased estimator although it has the desired characteristic of having a zero average bias.

The derivations in this section will be kept as general as possible and could be applied to any system independent of the specific window function used. However, the numerical calculations will be performed for the case of the rectangular window function. These calculations could easily be done for any window function if we were given the specifications of a particular system, but we have chosen to do them only for the rectangular case to minimize the number of computations which are already relatively extensive even for this latter case.

4.2 Cramér-Rao Bound

Using the model described in section 2.0, we will in this subsection present the Cramér-Rao bound for the estimation of the input signal frequency. To this end, we let

$$\bar{R} = \{r_1, r_2, r_3, \ldots, r_N\}$$

be the received vector where the r_i's are the pixel output values for a given integrated time frame. We can write

$$r_i = m_i(f_0, A) + n_i, \qquad i = 1, 2, 3, \ldots, N \tag{71}$$

where the n_i's are zero-mean, independent identically-distributed Gaussian random variables with variance σ^2, the m_i's are the signal components, N is the number of pixels in the photodetector array and f_0, A are respectively the frequency and amplitude of the input signal as defined in equation (3). This means that the conditional probability of the received vector $\bar{R}$ given that the frequency of the input signal is f_o is

$$p\left(\bar{R} \mid f_o\right) = \prod_{i=1}^{N} \frac{1}{\sqrt{2\pi}\sigma} \exp\left(\frac{-(r_i - m_i)^2}{2\sigma^2}\right) \tag{72}$$

where it is understood that the m_i's are the corresponding signal components for an input signal of frequency f_o and amplitude A. The Cramér-Rao bound [13, pp. 66] provides that

$$\mathrm{Var}[\hat{f}_o(\bar{R}) - f_o] \geq \left\{ E\left\{ \left[\frac{\partial \ln p(\bar{R} \mid f_o)}{\partial f_o}\right]^2 \right\} \right\}^{-1} \tag{73}$$

where $\hat{f}_o(\bar{R})$ is any unbiased estimate of f_o.

Taking the natural logarithm on both sides of equation (72) we get

$$\ln\left(p(\bar{R} \mid f_o)\right) = -N\ln(\sqrt{2\pi}\sigma) - \sum_{i=1}^{N} \frac{(r_i - m_i)^2}{2\sigma^2}, \tag{74}$$

so that

$$\frac{\partial \ln p(\bar{R} \mid f_o)}{\partial f_o} = \frac{1}{\sigma^2} \sum_{i=1}^{N} (r_i - m_i) m_i' \tag{75}$$

where $m_i' = \partial m_i / \partial f_o$. Squaring both sides of equation (75) we get

$$\left[\frac{\partial \ln p(\bar{R} \mid f_o)}{\partial f_o}\right]^2 = \frac{1}{\sigma^4}\left(\sum_{i=1}^{N}(r_i m_i' - m_i m_i')^2 + \sum_{i=1}^{N}\sum_{\substack{j=1\\j\neq i}}^{N}(r_i m_i' - m_i m_i')(r_j m_j' - m_j m_j')\right) \quad (76)$$

and expanding the terms of equation (76) we obtain

$$\left[\frac{\partial \ln p(\bar{R} \mid f_o)}{\partial f_o}\right]^2 = \frac{1}{\sigma^4}\sum_{i=1}^{N}(r_i^2(m_i')^2 + m_i^2(m_i')^2 - 2r_i m_i(m_i')^2$$

$$+ \frac{1}{\sigma^4}\sum_{i=1}^{N}\sum_{\substack{j=1\\j\neq i}}^{N}(r_i m_i' r_j m_j' - r_i m_i' m_j m_j' - m_i m_i' r_j m_j' + m_i m_i' m_j m_j'). \quad (77)$$

Now $E(r_i) = m_i$ and $E(r_j) = m_j$ and since r_i, r_j are independent provided that $i \neq j$, then

$$E(r_i r_j) = E(r_i)E(r_j) = m_i m_j.$$

Also, it is easy to show that $E(r_i^2) = \sigma^2 + m_i^2$. Using these identities and simplifying (77) we get that

$$E\left\{\left[\frac{\partial \ln p(\bar{R} \mid f_o)}{\partial f_o}\right]^2\right\} = \sum_{i=1}^{N}\frac{(m_i')^2}{\sigma^2}. \quad (78)$$

Combining equations (73) and (78) we get that the Cramér-Rao inequality for this problem is

$$\mathrm{Var}[\hat{f}_o(\bar{R}) - f_o] \geq \frac{\sigma^2}{\sum_{i=1}^{N}(m_i')^2}. \quad (79)$$

We have shown in section 2.0 that for a sinusoidal input $u(t) = A\cos(2\pi f_o t + \phi)$,

$$m_k = \frac{A^2 I}{4}\mathcal{H}(f_k - f_o) \quad (80)$$

where $\mathcal{H}(f)$ is the convolution between the functions $G(f)$ and $H(f)$

$$\mathcal{H}(f) = \int_{-\infty}^{\infty} H(f - f')G(f')df' \quad (81)$$

and

$$G(f) = \left|\int_{-\infty}^{\infty} w(t)\exp(-i2\pi ft)dt\right|^2. \quad (82)$$

As it was mentioned, we will use an $H(f)$ which is a rectangular function of unit amplitude and width B Hz symmetrical about $f = 0$ and a $w(t)$ which is a rectangular window whose duration is τ, the time taken for the acoustic wave to travel across the Bragg cell. For this case we have that

$$G(f) = \tau^2 \frac{\sin^2(2\pi f \tau/2)}{(2\pi f \tau/2)^2}. \tag{83}$$

Once we have obtained $\mathcal{H}(f)$ it becomes easy to calculate the outputs of the AOSA because these two are related as shown in equation (80). As an example, the signal components at the output of the AOSA are shown in Figure 16 and Figure 17. Figure 16 shows the signal components when $\tau B = 3/4$ and Figure 17 shows the signal components when $\tau B = 6$. Both of these figures show the output when f_o corresponds to one f_k as well as when f_o is exactly in the middle of two f_k's.

Using numerical differentiation we can calculate the variance of the efficient estimator, $\mathrm{Var}_{\mathrm{eff}}$ which is the equality case of equation (79). We are interested in knowing how the efficient estimator varies with τB and also how it varies as a function of the frequency f_o. In the latter case, we know that for a given τB the efficient estimator will be periodic with a period of B Hz provided that the frequency of the input signal does not correspond to a frequency near the edge of the array.

Obviously, the number of pixel values that we include in our calculations does not have to be N, which is the number of photodetectors in the array. The reason for this is that, for many of those pixels, the values of the m_i's are relatively small. Hence, we have included in our calculations as may pixels as was required but not more since this would increase the number of computations without any benefit, and we will call this number n. Using 55 pixels, we find that for $\tau B = 1/4$ the efficient estimator is quite constant as we vary the input frequency and

$$\sqrt{\mathrm{Var}_{\mathrm{eff}}} \approx 1.27 \frac{4\sigma}{\tau^2 A^2 I}$$

whereas for $\tau B = 1/2$ we find that it is also fairly constant except that in this case

$$\sqrt{\mathrm{Var}_{\mathrm{eff}}} = 0.98 \frac{4\sigma}{\tau^2 A^2 I}$$

where $\sqrt{\mathrm{Var}_{\mathrm{eff}}}$ is the root mean squared (RMS) error for the efficient estimator which we will henceforth call $\mathrm{RMS}_{\mathrm{eff}}$. Letting
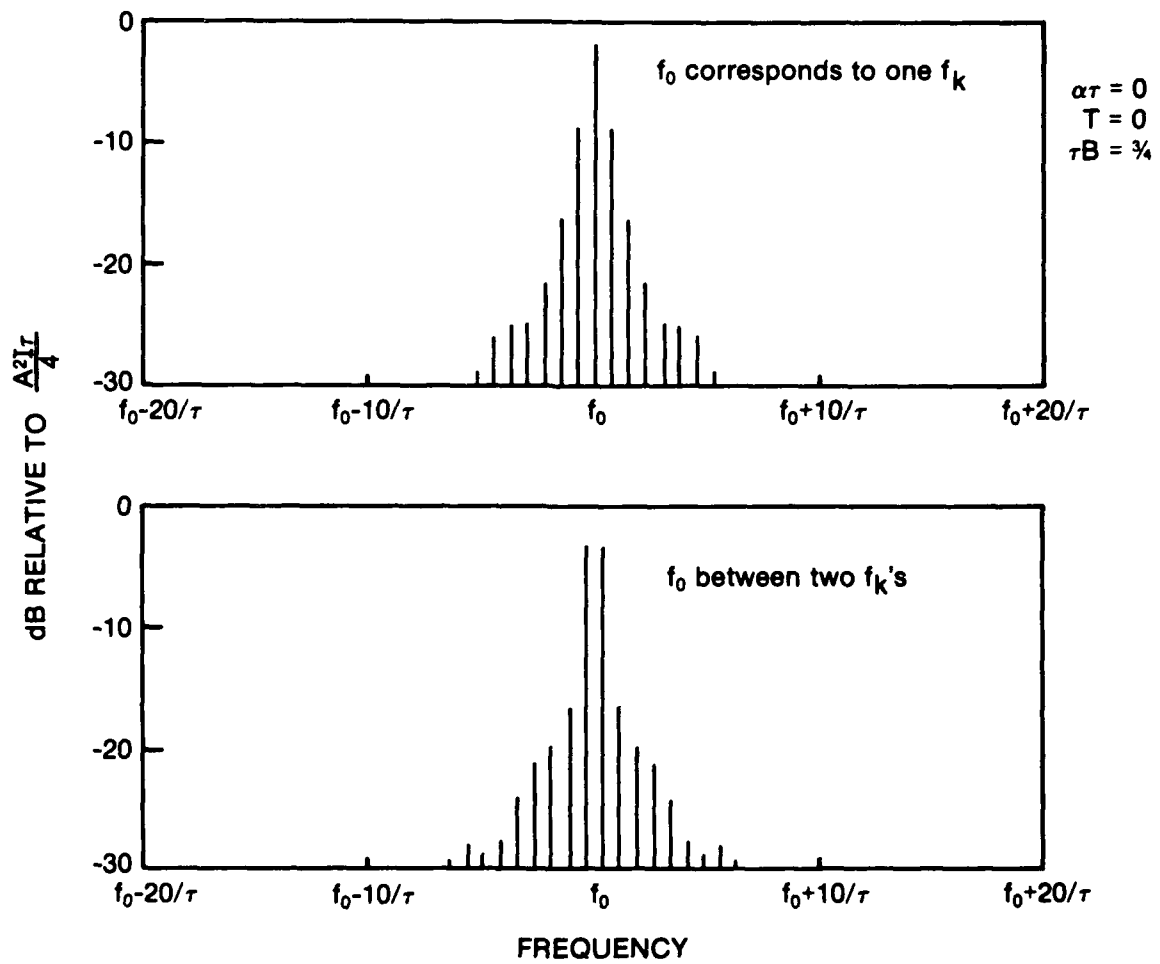
$$K = \frac{A^2 I \tau}{4\sigma}$$

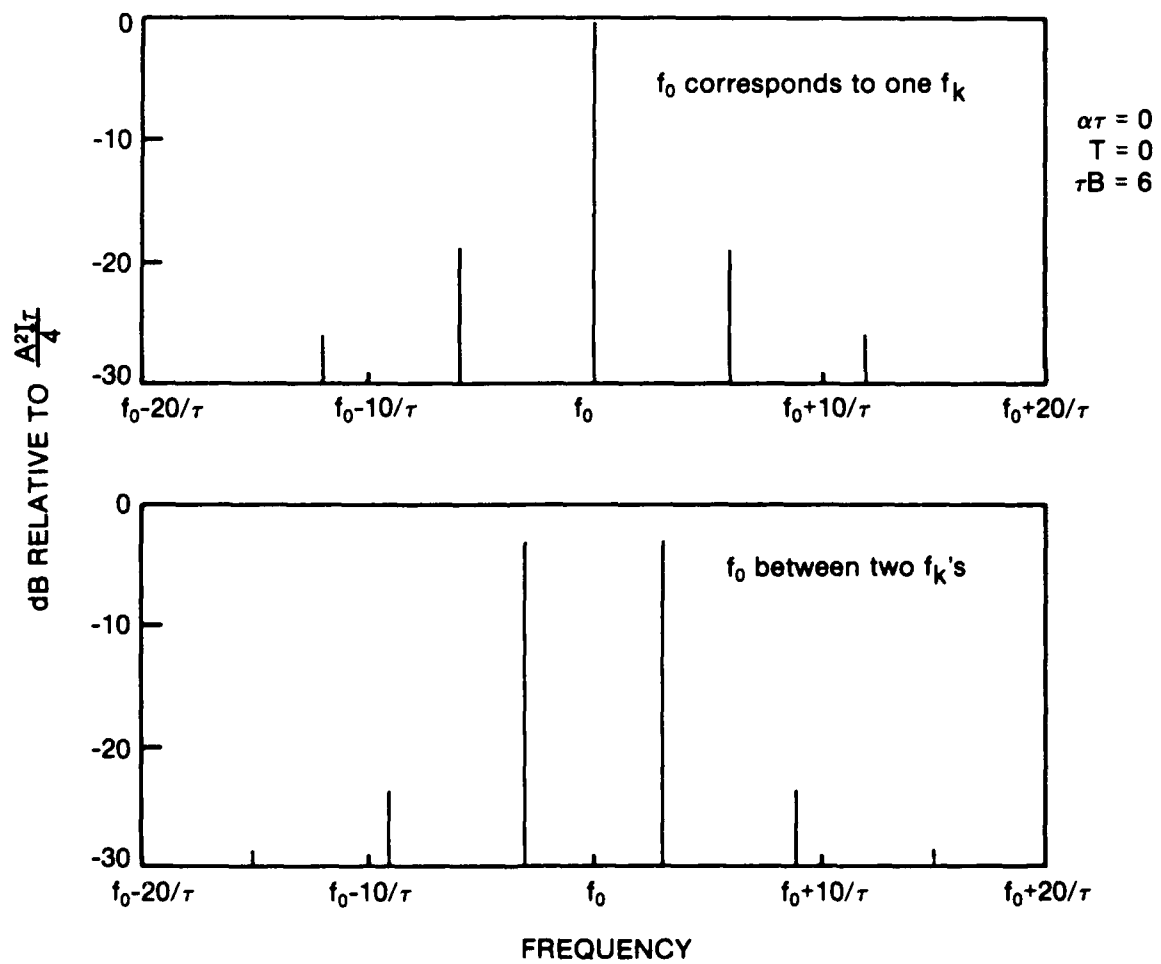FIGURE 16: OUTPUT OF AOSA FOR $\alpha\tau = 0$, $T = 0$, $\tau B = 3/4$

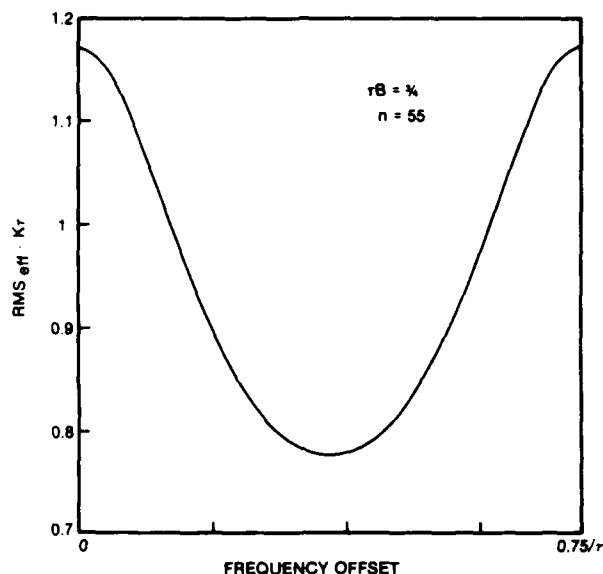FIGURE 17: OUTPUT OF AOSA FOR $\alpha\tau = 0$, $T = 0$, $\tau B = 6$

FIGURE 18: $\mathrm{RMS_{eff}}$ WHEN $\tau B = 3/4$

figures 18 to 22 show $\mathrm{RMS_{eff}}$ as a function of the frequency offset, which is the difference between the input frequency f_o and the corresponding frequency of the closest lower pixel. When f_o exactly corresponds to one of the f_k's then this frequency offset is zero. In these figures we have only plotted $\mathrm{RMS_{eff}}$ over one of its period because, as it was mentioned earlier $\mathrm{RMS_{eff}}$ as a function of frequency is periodic with period B Hz.

Since the input frequency f_o could be any frequency, it is interesting to know what is the average $\mathrm{RMS_{eff}}$. This can be done by averaging curves such as those in Figures 18 to 22. This has been done for several values of the constant τB and the result is as shown in Figure 23. We see from this curve that the average $\mathrm{RMS_{eff}}$ is relatively small when τB is between 0.25 and 1.25, but it increases exponentially as τB is closer to 2. Figure 24 demonstrates this more clearly as it shows the average $\mathrm{RMS_{eff}}$ for higher values of τB. It should be noted on this figure that the average $\mathrm{RMS_{eff}}$ for values of the constant τB in the proximity of 2, 3 and 4 are actually off scale. The actual value of the average $\mathrm{RMS_{eff}}$ for $\tau B = 3$ is $241/K\tau$ whereas for $\tau B = 2$ and 4 it is several orders of magnitude higher.

Since Figure 24 gives us a lower bound for any unbiased estimator, it is clear that any such estimator would have a very undesirable performance for τB greater than 1.75. In fact, we could even doubt that an unbiased estimator even exists for some of these values of τB.
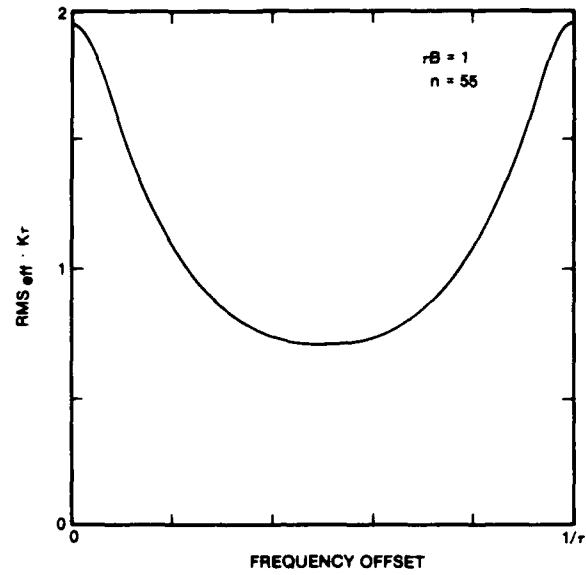
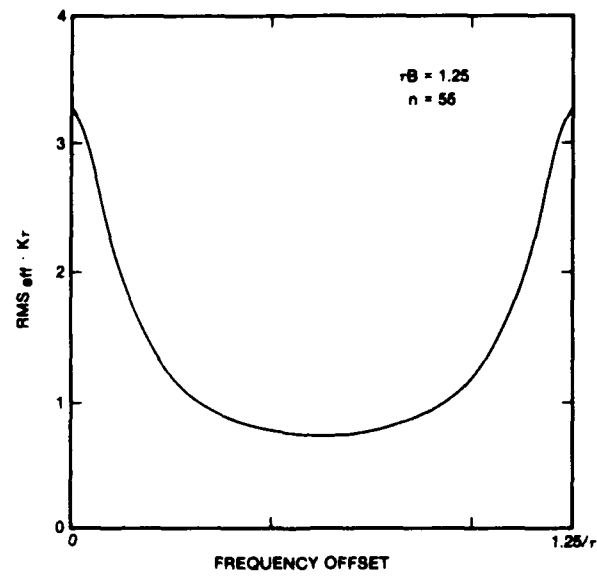FIGURE 19:   RMS$_{\text{eff}}$ WHEN $\tau B = 1$

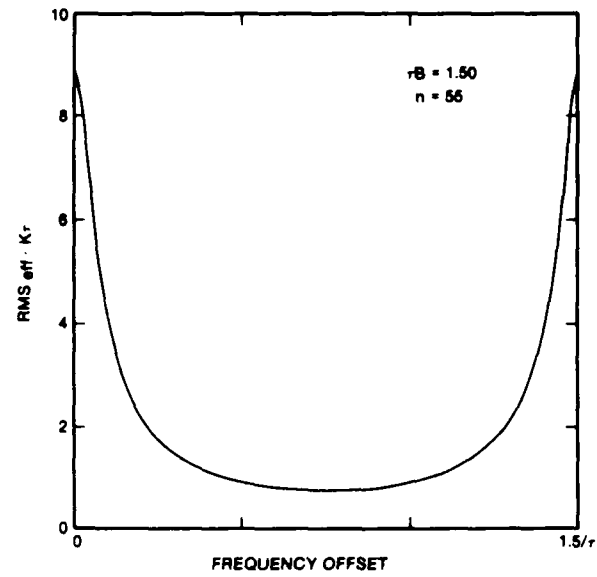FIGURE 20:   RMS$_{\text{eff}}$ WHEN $\tau B = 1.25$

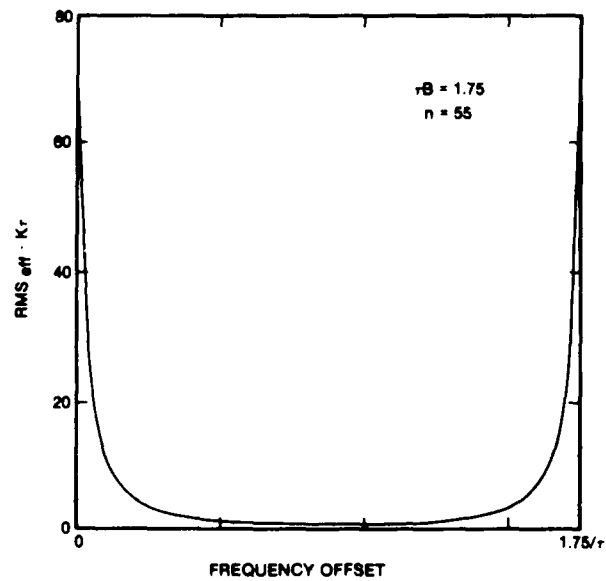FIGURE 21: RMS_{eff} WHEN $\tau B = 1.5$

FIGURE 22: RMS_{eff} WHEN $\tau B = 1.75$
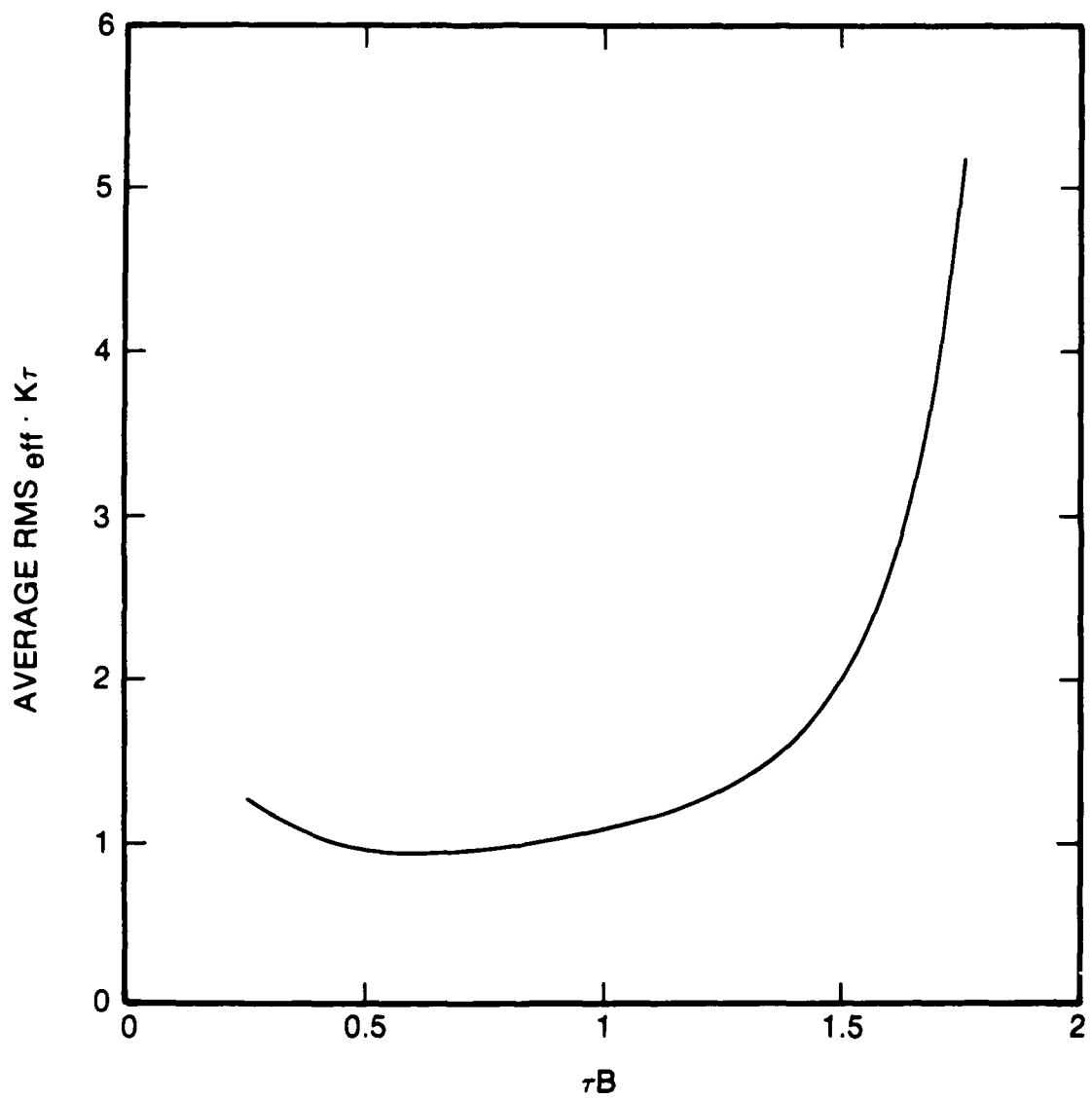
FIGURE 23: AVERAGE RMS ERROR OF THE EFFICIENT ESTIMATOR $(0 < \tau B < 2)$
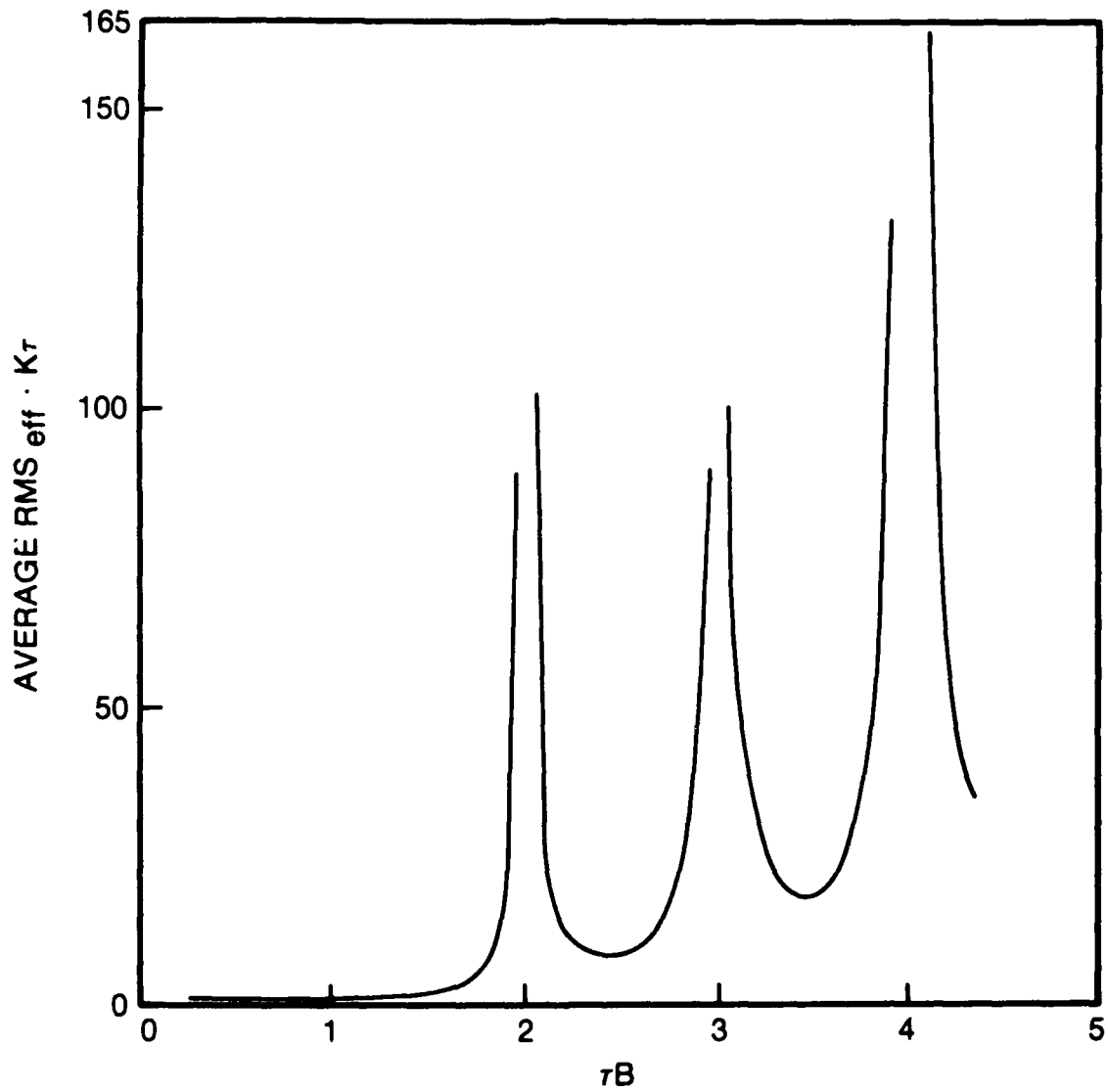
FIGURE 24:   AVERAGE RMS ERROR OF THE EFFICIENT ESTIMATOR
             $(0 < \tau B < 5)$

4.3 Peak-Detecting Estimator

In the previous subsection, we have presented the Cramér-Rao lower bound on the variance of any unbiased estimator for this problem. We have found that this bound increases exponentially as the value of the constant τB increases higher than 1.75 and that it even peaks at extremely high values in the vicinity of certain values of τB. This means that any unbiased estimator for this problem would have a poor performance for values of τB greater than 1.75 and, in fact it is probably impossible to find an unbiased estimator for this problem for some of these values of τB.

In this subsection, in an effort to find a solution to the frequency estimation problem, we present the performance of the peak-detecting estimator. That is, we present the performance of the algorithm that assumes that the frequency of the input signal is the frequency that corresponds to the highest pixel value. We want to investigate the performance of this estimator since it is very natural and simple to implement. In addition, it requires no modification for a different value of τB or for a different window function $w(t)$, and it works equally well on linear or logarithmic data.

We can let $X_1, X_2, X_3, \ldots, X_N$ be N independent Gaussian random variables with equal variance σ^2 for which the means are $\bar{X}_1, \bar{X}_2, \bar{X}_3, \ldots, \bar{X}_N$ respectively. This means that the probability density functions for these random variables are

$$f(x_i) = \frac{1}{\sigma\sqrt{2\pi}} \exp\left(\frac{-(x_i - \bar{X}_i)^2}{2\sigma^2}\right), \qquad i = 1, 2, 3, \ldots, N \tag{84}$$

and since these random variables are independent we can write their joint density function as

$$f(x_1, x_2, x_3, \ldots, x_N) = \frac{1}{(\sigma\sqrt{2\pi})^N} \prod_{i=1}^{N} \exp\left(\frac{-(x_i - \bar{X}_i)^2}{2\sigma^2}\right). \tag{85}$$

If we define Ψ_j as the probability that the random variable X_j is larger than all the others, then it can be evaluated by the following N integrals

$$\Psi_j = p(X_i < X_j, \qquad \forall i \neq j)$$

$$= \int_{-\infty}^{\infty} \overbrace{\int_{-\infty}^{x_j} \int_{-\infty}^{x_j} \int_{-\infty}^{x_j} \cdots \int_{-\infty}^{x_j}}^{(N-1)\ \text{times}} f(x_1, x_2, x_3, \ldots, x_N)$$

$$dx_1 dx_2 dx_3 \cdots dx_{j-1} dx_{j+1} \cdots dx_N dx_j \tag{86}$$

which through a change of variables can be rewritten

$$\Psi_j = \int_{-\infty}^{\infty} \frac{1}{\sigma\sqrt{2\pi}} \exp\left(\frac{-(x_j - \bar{X}_j)^2}{2\sigma^2}\right) \prod_{\substack{i=1 \\ i \neq j}}^{N} \left(\frac{1}{2}\left[1 + \mathrm{erf}\left(\frac{x_j - \bar{X}_i}{\sqrt{2}\sigma}\right)\right]\right) dx_j \tag{87}$$

where

$$\mathrm{erf}(y) = \frac{2}{\sqrt{\pi}} \int_0^y \exp(-t^2)dt. \tag{88}$$

Using equation (87) we get the RMS error for the peak-detecting estimator

$$\mathrm{RMS_{pk}} = \sqrt{\sum_{j=1}^{N}(f_j - f_o)^2 \Psi_j} \tag{89}$$

and also the mean error for this estimator

$$\mathrm{Mean_{pk}} = \sum_{j=1}^{N}(f_j - f_o)\Psi_j. \tag{90}$$

Figures 25 and 26 show $\mathrm{RMS_{pk}}$ and $\mathrm{Mean_{pk}}$ respectively for the case of $\tau B = 0.5$, $n = 15$, and $K = A^2 I\tau/4\sigma = 10$.

FIGURE 25: RMS ERROR OF THE PEAK-DETECTING ESTIMATOR
($\tau B = 0.5$, $n = 15$, $K = 10$)

Figures 27 and 28 show $\mathrm{RMS_{pk}}$ and $\mathrm{Mean_{pk}}$ respectively for the same case except for $K = 20$. Again in these figures we have plotted only one period of these functions since they are periodic with period B Hz.

FIGURE 26:   MEAN ERROR OF THE PEAK-DETECTING ESTIMATOR
$(\tau B = 0.5,\ n = 15,\ K = 10)$

FIGURE 27:   RMS ERROR OF THE PEAK-DETECTING ESTIMATOR
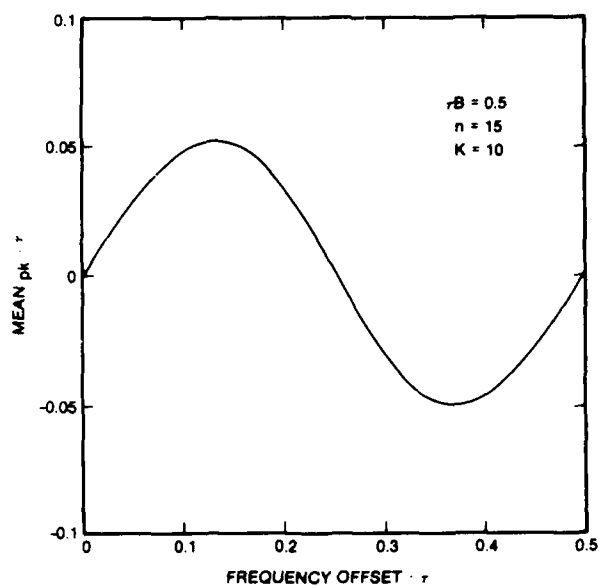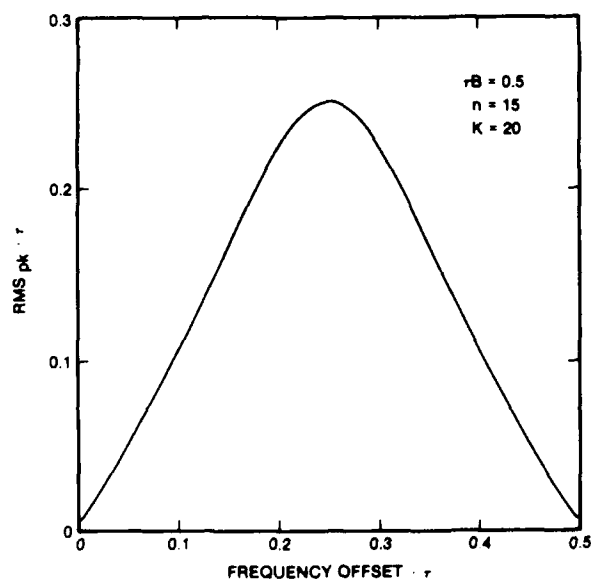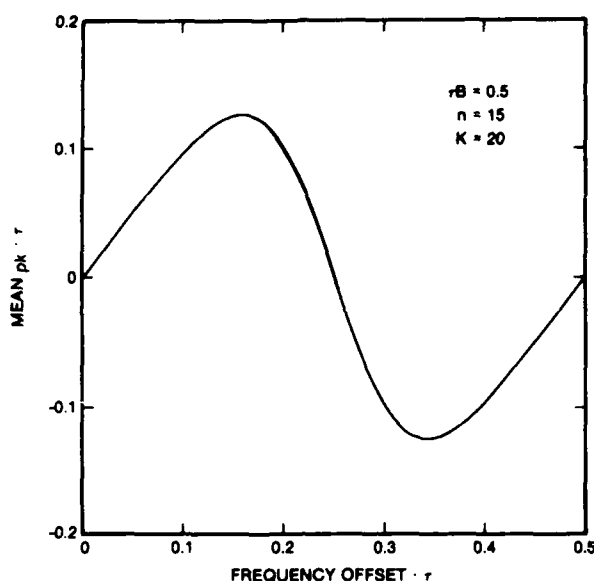$(\tau B = 0.5,\ n = 15,\ K = 20)$

FIGURE 28:   MEAN ERROR OF THE PEAK-DETECTING ESTIMATOR
($\tau B = 0.5$, $n = 15$, $K = 20$)

We see from figures 26 and 28 that the peak-detecting estimator is actually a biased estimator of the input frequency. However, it has the desired characteristic of having a zero average bias over many different input frequencies. This can be seen by the symmetry of figures 26 and 28.

As we have done with the Cramér-Rao bound, we can obtain the average $\mathrm{RMS_{pk}}$ by averaging curves such as those of figures 25 and 27. This has been done for several values of the constant τB for a given K. Figure 29 shows the resulting family of curves for several values of K. These curves have all been obtained by assuming 15 photodetectors in our calculations (i.e. $n = 15$) so that we could compare the performance from a common basis. It should be noted that, for any given value of K there is a value of τB which is really the smallest that would be used in practice. This is because the signal is so buried in the noise that the corresponding false alarm rate would be exceedingly high. We have not plotted points beyond that point on Figure 29. We see from that figure that the smallest useful τB increases as we decrease the value of K, which is in fact related to the signal to noise ratio (i.e. $K = A^2 I\tau/4\sigma$). We also see from Figure 29 that for any given value of K, there is an optimum τB which gives the smallest RMS error. As in the case of the smallest useful τB, we see that this optimum τB increases as the value of K decreases.

Finally, we note from Figure 29 that for any value of K the average RMS error for the peak-detecting estimator asymptotically tends towards a straight line as we increase the value of τB. So that we can see this better, we have plotted a straight line

FIGURE 29:   AVERAGE RMS ERROR OF THE PEAK-DETECTING ESTIMATOR

on Figure 29 that has a slope of $0.25/\tau$ and that passes through the origin.

This behaviour is to be expected and to see why let us consider the case of no noise or infinite signal to noise ratio. Figures 30 and 31 show the RMS error and the mean error (or the bias) of the peak-detecting estimator for this latter case. It is easy to see that the average RMS error in that case is $B/4$ and hence if $\tau B = a$, then the average RMS error will be $B/4 = a/4\tau$ which is in agreement with Figure 29.

FIGURE 30: RMS ERROR OF THE PEAK-DETECTING ESTIMATOR WHEN $K = \infty$

FIGURE 31:   MEAN ERROR (BIAS) OF THE PEAK-DETECTING ESTIMATOR WHEN
WHEN $K = \infty$

5.0   ESTIMATION OF THE POWER

5.1   Introduction

Another important signal parameter of interest when monitoring the
electromagnetic environment is the received signal power. This information can
be used to analyze the scan pattern of the transmitter or to obtain a gross estimate
of the distance to the emitter. In certain system configurations, the power estimate is
used for direction finding and in any case we can know if the emitter is approaching or
receding by comparing its relative power in consecutive time frames.

Since we have no knowledge of the a priori probabilities for the power of the input
signals, we are dealing with a nonrandom parameter estimation problem. This means
that we will have to work with the a posteriori density functions.

In this section, we will also assume that the power estimation is a secondary task to the frequency estimation. That is, we will assume that the frequency estimation of the signal has been done prior to the estimation of its power. This added information will allow us to get a better estimation of the power and it will insure that we associate one power estimation with one frequency estimation. The latter statement will be especially important if, because of the system configuration used the energy of the input signal spreads over several pixels.

Even though there are no general results on how to achieve an optimal estimator for the nonrandom estimation situation, one estimator which is often used for these cases is the maximum likelihood (ML) estimator. This estimator is based on the maximum likelihood principle and more specifically it consists in choosing as our estimate the value of the parameter that most likely caused the given value of the received signal.

An important property of the maximum likelihood estimator is that if it is unbiased (i.e. the expected value of the estimate is equal to the true value of the parameter of interest) then it will satisfy the Cramér-Rao lower bound with an equality [14]. Any unbiased estimate that satisfies this bound with an equality is called an *efficient* estimate because it is impossible to find any other unbiased estimate with a lower variance.

In the next subsection we present the ML estimate of the power of the input signal assuming that the input signal frequency f_o is known. We also analyze the expectation and the variance of this estimate. In the third subsection of this section, we analyze the effects of inaccuracies in our estimate of f_o on this ML estimate since in practice f_o would not be known, but would have to be estimated.

5.2 Maximum Likelihood Estimate

Using the model presented in section 2.0, we will in this section present the ML estimate of the input signal power. To this end, we let

$$\bar{R} = \{r_1, r_2, r_3, \ldots, r_N\}$$

be the received vector where the r_i's are the pixel output values for a given frame. We can write

$$r_i = m_i(f_0, A) + n_i, \qquad i = 1, 2, 3, \ldots, N \tag{91}$$

where the n_i's are zero-mean, independent identically-distributed Gaussian random variables with variance σ^2, the m_i's are the signal components, N is the number of pixels in the photodetector array and f_0, A are respectively the frequency and amplitude of the input signal as defined in equation (3).

We will assume that the frequency f_o of the input signal is known and will let $S = A^2$ be the parameter to estimate. This means that the conditional probability of the received vector $\bar{R}$ given that the squared amplitude of the input signal is S will be

$$p(\bar{R} \mid f_o, S) = \prod_{i=1}^{N} \frac{1}{\sqrt{2\pi\sigma^2}} \exp\left[\frac{-(r_i - m_i)^2}{2\sigma^2}\right] \tag{92}$$

where it is understood that the m_i's are the corresponding signal components for an input signal of frequency f_o and amplitude A.

Now to find the ML estimate of A^2 we must solve

$$\frac{\partial \ln\{p(\bar{R} \mid S, f_o)\}}{\partial S} = 0. \tag{93}$$

Substituting equation (92) in equation (93) and simplifying gives us

$$\frac{\partial \sum_{i=1}^{N} (r_i - m_i)^2 / 2\sigma^2}{\partial S} = 0. \tag{94}$$

Substituting for the m_i's as in equation (22) and simplifying we get

$$\frac{\partial \sum_{i=1}^{N} \left(\frac{SI}{4} \mathcal{H}_i - r_i\right)^2}{\partial S} = 0. \tag{95}$$

Differentiating and simplifying we obtain

$$\sum_{i=1}^{N} \left(\frac{I\mathcal{H}_i^2}{4} S - r_i \mathcal{H}_i\right) = 0 \tag{96}$$

from which we get the desired ML estimate

$$\hat{S}_{\text{ML}} = \frac{4}{I} \frac{\sum_{i=1}^{N} r_i \mathcal{H}_i}{\sum_{i=1}^{N} \mathcal{H}_i^2}. \tag{97}$$

If we seek to find the mean of the ML estimate, we have that

$$E\{\hat{S}_{\text{ML}}\} = E\left\{\frac{4 \sum_{i=1}^{N} r_i \mathcal{H}_i}{I \sum_{i=1}^{N} \mathcal{H}_i^2}\right\} \tag{98}$$

which becomes

$$E\{\hat{S}_{\mathrm{ML}}\} = \frac{4}{I\sum_{i=1}^{N}\mathcal{H}_i^2}\sum_{i=1}^{N}\mathcal{H}_i E\{r_i\} \tag{99}$$

which can easily be calculated to be

$$E\{\hat{S}_{\mathrm{ML}}\} = A^2 = S. \tag{100}$$

Hence we see that $\hat{S}_{\mathrm{ML}}$ is an unbiased estimate of the parameter A^2. This is a very important result because it means that $\hat{S}_{\mathrm{ML}}$ is an efficient estimate of A^2 and thus it is impossible to find another unbiased estimate of A^2 which has a smaller variance than the ML estimate of A^2.

If we seek to find the variance of $\hat{S}_{\mathrm{ML}}$, from equation (97) we have

$$\mathrm{Var}(\hat{S}_{\mathrm{ML}}) = \mathrm{Var}\left(\frac{4}{I}\frac{\sum_{i=1}^{N}r_i\mathcal{H}_i}{\sum_{i=1}^{N}\mathcal{H}_i^2}\right) \tag{101}$$

but since the r_i's are independent random variables we have that

$$\mathrm{Var}(\hat{S}_{\mathrm{ML}}) = \frac{16}{I^2(\sum_{i=1}^{N}\mathcal{H}_i^2)^2}\sum_{i=1}^{N}\mathcal{H}_i^2\mathrm{Var}(r_i) \tag{102}$$

and since $\mathrm{Var}(r_i) = \sigma^2$ for all i we get

$$\mathrm{Var}(\hat{S}_{\mathrm{ML}}) = \frac{16\sigma^2}{I^2(\sum_{i=1}^{N}\mathcal{H}_i^2)}. \tag{103}$$

In Appendix I we have tabulated values of $\sum_{i=1}^{N}\mathcal{H}_i^2$ for different τB. From Table I-1 and from equation (103) we can see how the system design parameters affect the variance of the ML estimate of the input signal power. We see that the integration time of the photodetectors I and the Bragg cell aperture time τ are two strong parameters. Increasing either of these parameters will reduce the variance in a square law relationship. Increasing the value of τB will reduce the variance according to the relationship shown in Appendix I. Of course, if we reduce the noise variance we will also reduce the variance of the ML estimate and this is a direct linear relationship.

5.3   Effect of Inaccuracies in the Frequency Estimate

In the previous subsection we obtained the ML estimate of the input signal power. We saw that the ML estimate is unbiased in this case and this therefore implies that it is an *efficient* estimate. This means that it is impossible to find another unbiased estimate of A^2 which has a smaller variance than the ML estimate of A^2.

However, these results were obtained under the assumption that the frequency of the input signal f_o was known. In practice, f_o would not be known but would have to be estimated. This means that there might be inaccuracies in our estimate of f_o. In this subsection, we analyze the effects of these inaccuracies on the ML estimate of the power that we obtained in the previous subsection.

To this end, let

$$\tilde{S} = \frac{4}{I} \frac{\sum_{i=1}^{N} r_i \tilde{\mathcal{H}}_i}{\sum_{i=1}^{N} \tilde{\mathcal{H}}_i^2} \tag{104}$$

be our estimate of A^2 where the $\tilde{\mathcal{H}}_i$'s correspond to frequency $\tilde{f}_o$ which could be different from f_o. Equation (104) is the same as the ML estimate algorithm of equation (97) except that it uses the $\tilde{\mathcal{H}}_i$'s instead of the $\mathcal{H}_i$'s to take into account the fact that our estimate of the input signal frequency $\tilde{f}_o$ could be different from the actual input signal frequency f_o.

We are interested in knowing how inaccuracies in the input signal frequency will affect the mean of the estimator defined by equation (104). To obtain this information, we can take the mean on both sides of this equation

$$E\{\tilde{S}\} = E\left\{ \frac{4}{I} \frac{\sum_{i=1}^{N} r_i \tilde{\mathcal{H}}_i}{\sum_{i=1}^{N} \tilde{\mathcal{H}}_i^2} \right\} \tag{105}$$

which becomes

$$E\{\tilde{S}\} = \frac{4}{I \sum_{i=1}^{N} \tilde{\mathcal{H}}_i^2} \sum_{i=1}^{N} \tilde{\mathcal{H}}_i E\{r_i\} \tag{106}$$

which after substitution and simplification becomes

$$E\{\tilde{S}\} = A^2 \frac{\sum_{i=1}^{N} \mathcal{H}_i \tilde{\mathcal{H}}_i}{\sum_{i=1}^{N} \tilde{\mathcal{H}}_i^2}. \tag{107}$$

Hence, we see from equation (107) that the estimator of the power defined by equation (104) is no longer unbiased when $\tilde{f}_o$ is different from f_o. If we let $\tilde{f}_o$ correspond

to an f_k, which would be the case if we were using the peak-detecting estimator, then the resulting bias would be as shown in Figure 32, where we have assumed rectangular windowing. This figure shows the resulting normalized bias for different values of τB which represent different system configurations. We have not included the curves for $\tau B = 3/4$ and $\tau B = 1/2$ on that figure since they represent very little variation from the curve for $\tau B = 1$.

An important observation to make concerning Figure 32 is that inaccuracies in the estimation of the input frequency will, on the average, cause us to under estimate the power of the input signal if we use the estimator of equation (104). Small inaccuracies in the estimation of the frequency will have negligible effects, but inaccuracies greater than a certain value will have considerable effects.

It is clear from Figure 32 that larger values of τB present more robustness to small inaccuracies in the estimation of the frequency. However, as it was shown in section 4.0, larger values of τB will also on the average cause us to make larger errors in the estimation of the frequency thereby diminishing the advantage of larger values of τB. In Table 1, we have tabulated the normalized bias of the ML estimator when the frequency inaccuracy is half a pixel, for different values of τB. We can see from this table that for the larger values of τB (2,3,4), inaccuracies in the estimator of the frequency of only half a pixel will cause us on the average to under estimate the power of the input signal by almost 50% if we use the estimator of equation (104).

τB	$(f_0 - \tilde{f}_0)\tau$	$E\{\tilde{s}\}/A^2$
0.5	± 0.25	0.90
0.75	± 0.375	0.77
1	± 0.5	0.63
2	± 1	0.54
3	± 1.5	0.53
4	± 2	0.52

TABLE 1.   NORMALIZED BIAS OF ML ESTIMATOR WHEN $(f_0 - \tilde{f}_0) = \pm B/2$

We are also interested in knowing how inaccuracies in the input signal frequency will affect the variance of the estimator defined by equation (104). To obtain this information, we can take the variance on both sides of this equation

$$\mathrm{Var}(\tilde{S}) = \mathrm{Var}\left(\frac{4}{I} \frac{\sum_{i=1}^{N} r_i \tilde{\mathcal{H}}_i}{\sum_{i=1}^{N} \tilde{\mathcal{H}}_i^2} \right)$$

$$= \frac{16}{I^2} \sigma \frac{\sum_{i=1}^{N} \tilde{\mathcal{H}}_i^2}{\left(\sum_{i=1}^{N} \tilde{\mathcal{H}}_i^2 \right)^2}$$
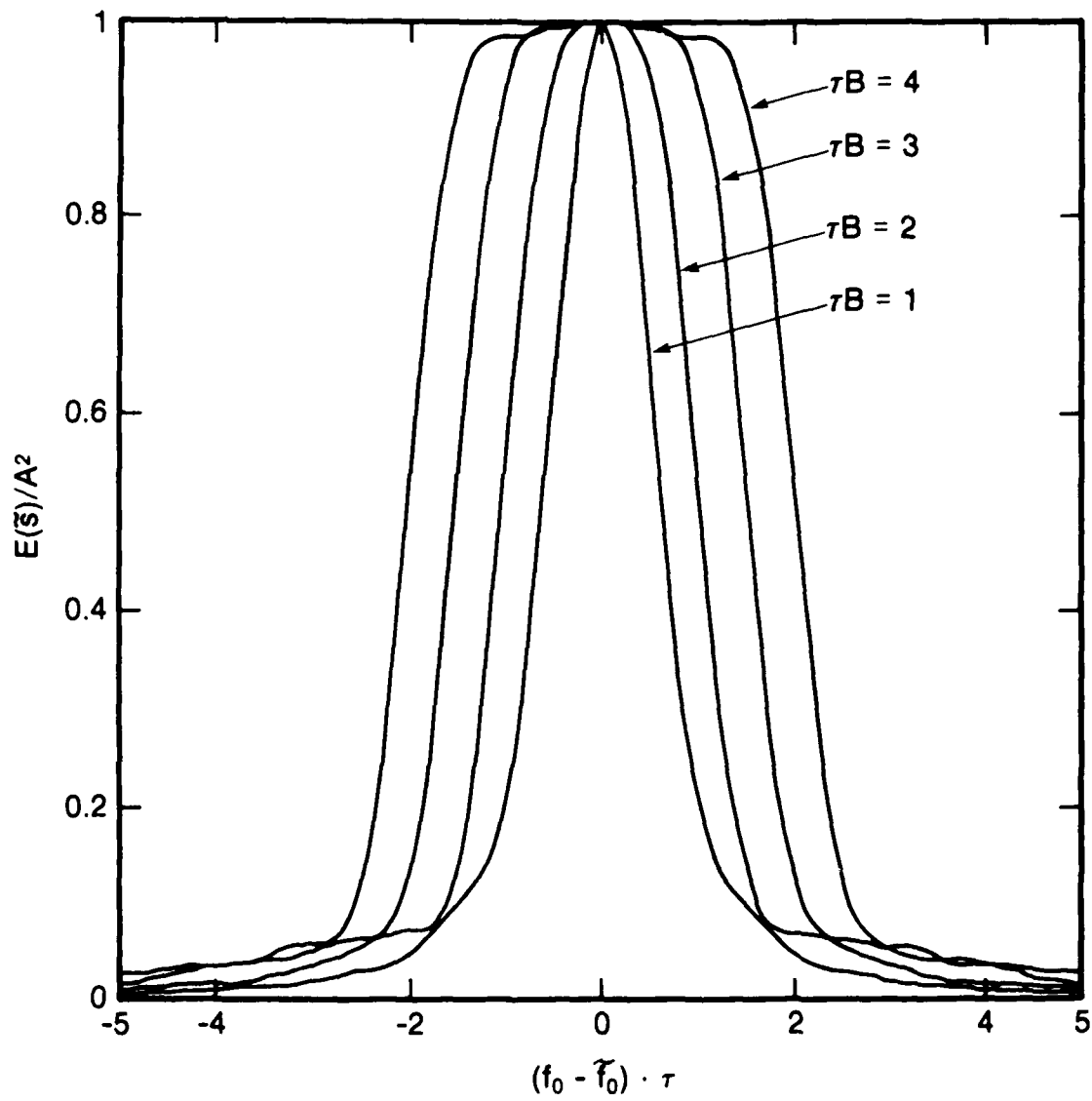
FIGURE 32:   NORMALIZED BIAS OF THE ML ESTIMATOR

and hence

$$\text{Var}(\tilde{S}) = \frac{16}{I^2} \frac{\sigma^2}{\sum_{i=1}^{N} \tilde{\mathcal{H}}_i^2}. \tag{108}$$

Referring to Appendix I, we see that inaccuracies in our estimate of the input signal frequency for the application of the estimator defined by equation (104) could either increase or decrease the variance of this estimator depending on what f_o and $\tilde{f}_o$ are relative to an f_k. For example, if we use the peak-detecting estimator to estimate the input signal frequency, then the variance of the estimator of equation (104) can only be smaller or equal to the variance of the ML estimator defined in equation (97). In fact, for that case if the input signal frequency is exactly between two f_k's then the estimator of equation (104) will have a smaller variance than the ML estimator and this effect will be more pronounced for larger values of τB.

Hence, we can conclude that the estimator of the input signal power defined by equation (104) performs well if the inaccuracy in the estimation of f_o is small. However, if this inaccuracy is larger than a certain amount, then this estimator could under estimate A^2 considerably. The variance of (104) could be larger or smaller than the variance of the ML estimator, but this effect is not as important as the bias error.

6.0 CONCLUSIONS AND COMMENTS

6.1 Summary

We have presented a statistical model of the output signals from an acousto-optic spectrum analyzer (AOSA) for the case where we are receiving continuous-wave (CW) signals. Using this model, we have shown that the optimum algorithm for the detection of a signal of known frequency is a discrete matched filter. In an effort to extend this algorithm to the case of the detection of an unknown frequency, we have proposed a sliding matched filter structure which can be implemented as a finite impulse response (FIR) filter. We have investigated the performance of such a scheme and have found it to be quite acceptable.

We also considered the frequency estimation problem by calculating the Cramér-Rao bound which is a lower bound for the variance of any unbiased estimator of the frequency. We saw that this bound had very undesirable characteristics for $\tau B > 1.75$ therefore indicating the undesirability of using an unbiased estimator for these cases. In an effort to find a solution to this problem, we presented the peak-detecting estimator and we investigated its performance. We saw that the peak-detecting estimator is a biased estimator although it has the desired characteristic of having a zero average bias, and we saw that its variance is relatively well behaved.

Finally, we considered the problem of estimating the power of the input signal. We found it convenient to approach this problem by letting the power estimation be a

secondary task to the frequency estimation. That is, we assumed that the frequency estimation of a signal would always be done prior to the power estimation of that signal. Under this assumption, we obtained the maximum likelihood (ML) estimator of the input signal power and showed that it was in fact an *efficient* estimator, which means that one cannot find another unbiased estimator with a lower variance. We investigated how errors in our estimate of the frequency would affect the ML algorithm, and we found that it would always cause us to underestimate the power of the input signal. For large errors, we saw that the underestimation could be quite serious. These errors in the estimation of the frequency were also found to affect the variance of the ML estimator but for the case when we are using the peak-detecting estimator, we saw that these errors would actually reduce the variance of the ML algorithm.

6.2 Suggestions for Further Research and Comments

The statistical analyses performed in this report were based on a system model which was defined in section 2.0. However, since the field of acousto-optics is relatively recent, we are still in the process of discovering new architectures which can have certain advantages depending on the application. The system model for these new architectures could be different from the one we have used and it would certainly be worthwhile to redo our statistical analyses for these other systems.

As we stated in section 2.0, all our numerical calculations were done with the assumption that the window function $w(t)$ was a rectangular function, although we mentioned how this function could be modified to account for some other practical issues of the AOSA such as the attenuation of the acoustic wave or the profile of the laser beam. It would certainly be worthwhile to redo our calculations for other system configurations especially if we had some reasons to be interested in a specific system design.

Finally, we have only analyzed the case when we are receiving a CW signal although we mentioned that an EW receiver would have to deal with many different types of signals. Perhaps the most important type of signal which could be analyzed is pulse modulated signals including those with complex modulation within the pulse. These signals are more complex since they present a larger number of parameters to be analyzed each one of which possibly exhibiting a large variation from one transmitter to the next. It is hoped that this report has contributed to a better understanding of the critical issues and tradeoffs that are involved and can therefore provide a basis for the development of an optimal or suboptimal solution to this more complex problem.

7.0 REFERENCES

[1] Tsui, James Bao-yen, *Microwave Receivers and Related Components*, National Technical Information Service, Springfield, 1983.

[2] Hamilton, M. C., Wille, D. A., Miceli, W. J., 'An Integrated Optical RF Spectrum Analyzer', IEEE Ultrasonics Symposium, October 1976.

[3] Wiley, Richard G., *Electronic Intelligence: the Analysis of Radar Signals*, Artech House, Dedham, 1982.

[4] Adler, Robert, 'Interaction Between Light and Sound', *IEEE Spectrum*, pp.42-54, May 1967.

[5] Lee, Jim Pak-Yee, *Acoustooptic Fourier Transforming Configuration For Spectrum Analysis and Determination of Direction-Of-Arrival*, P.H.d Thesis, Carleton University, August 1986.

[6] Goodman, Joseph W., *Introduction to Fourier Optics*, McGraw-Hill, 1968.

[7] Lee, Jim P.Y., 'Acoustooptic Spectrum Analysis of Radar Signals Using an Integrating Photodetector Array', *Applied Optics*, Vol. 20, No. 4, pp. 595-600, February 15, 1981.

[8] Kellman, Peter, et. al., 'Integrating Acousto-Optic Channelized Receivers', *Proceedings of the IEEE*, Vol. 69, No. 1, pp. 93-100, January 1981.

[9] Harms, B.K. and Hummels, D.R., 'Analysis of Detection Probability for the Acoustooptic Receiver', *IEEE transactions on Aerospace and Electronic Systems*, Vol. AES-22, No. 4, pp. 326-339, July 1986.

[10] Hecht, D.L., 'Spectrum Analysis Using Acousto-Optic Devices', *Optical Engineering*, Vol. 16, No. 5, pp. 461-466, September/October 1977.

[11] Heideman, Michael T., et. al., 'Gauss and the History of the Fast Fourier Transform', *IEEE ASSP Magazine*, Vol. 1, No. 4, pp. 14-21, October 1984.

[12] Farley, Guy and Hage, M., 'Dark Noise Characterization of a 25-Element Avalanche Photodiode Array' (U), Technical Memorandum, *DREO TM 86-29*, November 1986.

[13]   Van Trees, Harry L., *Detection, Estimation, and Modulation Theory, Part I*, Wiley, New York, 1968.

[14]   Haykin, S., et. al., *Array Signal Processing*, pp. 208, Prentice-Hall, 1984.

APPENDIX I

$\sum_{i=1}^{N} \mathcal{H}_i^2 / \tau^2$ FOR DIFFERENT VALUES OF τB

In this Appendix we have tabulated a few values of the expression $\sum_{i=1}^{N} \mathcal{H}_i^2$ for different values of τB since this expression appears in the performance calculations for the detection in section 3.0 and in the variance calculations of the maximum likelihood estimator for the power estimation in section 5.0. It should be noted that the result of this summation is a periodic function of period B as we vary the input signal frequency. We have used 25 terms to obtain these results since the remaining terms were insignificantly small and we have assumed rectangular windowing. Two cases have been considered, one where the input signal frequency f_0 corresponds to one of the f_k's of equation (22) and the other where f_0 is exactly between two f_k's. The former case represents a maximum for a given value of τB while the latter represents a minimum. The results of these calculations are shown in Table I-1.

τB	$\sum_{i=1}^{N} \mathcal{H}_i^2/\tau^2$	
	f_0 corresponds to one f_k	f_0 between two f_k's
0.25	0.163	0.163
0.50	0.308	0.308
0.75	0.452	0.396
1.00	0.611	0.409
1.25	0.730	0.415
1.50	0.792	0.434
1.75	0.814	0.449
2.00	0.817	0.452
3.00	0.868	0.467
4.00	0.903	0.475
5.00	0.920	0.480
6.00	0.934	0.483

TABLE I-1: $\sum_{i=1}^{N} \mathcal{H}_i^2/\tau^2$ FOR DIFFERENT VALUES OF τB

DOCUMENT CONTROL DATA

(Security classification of title, body of abstract and indexing annotation must be entered when the overall document is classified)

1. ORIGINATOR (the name and address of the organization preparing the document. Organizations for whom the document was prepared, e.g. Establishment sponsoring a contractor's report, or tasking agency, are entered in section 8.) DEFENCE RESEARCH ESTABLISHMENT OTTAWA NATIONAL DEFENCE SHIRLEY BAY, OTTAWA, ONTARIO K1A 0Z4 CANADA	2. SECURITY CLASSIFICATION (overall security classification of the document, including special warning terms if applicable) UNCLASSIFIED

3. TITLE (the complete document title as indicated on the title page. Its classification should be indicated by the appropriate abbreviation (S,C,R or U) in parentheses after the title.)

A STATISTICAL ANALYSIS OF THE OUTPUT SIGNALS OF AN ACOUTO-OPTIC SPECTRUM ANALYZER FOR CW SIGNALS (U)

4. AUTHORS (Last name, first name, middle initial. If military, show rank, e.g. Doe, Maj. John E.)

FARLEY, GUY, J.

5. DATE OF PUBLICATION (month and year of publication of document) OCTOBER 1988	6a. NO. OF PAGES (total containing information. Include Annexes, Appendices, etc.) 70	6b. NO. OF REFS (total cited in document) . 14

6. DESCRIPTIVE NOTES (the category of the document, e.g. technical report, technical note or memorandum. If appropriate, enter the type of report, e.g. interim, progress, summary, annual or final. Give the inclusive dates when a specific reporting period is covered.)

DREO REPORT

8. SPONSORING ACTIVITY (the name of the department project office or laboratory sponsoring the research and development. Include the address.)

9a. PROJECT OR GRANT NO. (if appropriate, the applicable research and development project or grant number under which the document was written. Please specify whether project or grant) 011LB11	9b. CONTRACT NO. (if appropriate, the applicable number under which the document was written)

10a. ORIGINATOR'S DOCUMENT NUMBER (the official document number by which the document is identified by the originating activity. This number must be unique to this document.) DREO REPORT 993	10b. OTHER DOCUMENT NOS. (Any other numbers which may be assigned this document either by the originator or by the sponsor)

11. DOCUMENT AVAILABILITY (any limitations on further dissemination of the document, other than those imposed by security classification)

  XX) Unlimited distribution
  ( ) Distribution limited to defence departments and defence contractors; further distribution only as approved
  ( ) Distribution limited to defence departments and Canadian defence contractors; further distribution only as approved
  ( ) Distribution limited to government departments and agencies; further distribution only as approved
  ( ) Distribution limited to defence departments; further distribution only as approved
  ( ) Other (please specify):

12. DOCUMENT ANNOUNCEMENT (any limitation to the bibliographic announcement of this document. This will normally correspond to the Document Availability (11). However, where further distribution (beyond the audience specified in 11) is possible, a wider announcement audience may be selected.)

UNCLASSIFIED

SECURITY CLASSIFICATION OF FORM

13 ABSTRACT (a brief and factual summary of the document. It may also appear elsewhere in the body of the document itself. It is highly
desirable that the abstract of classified documents be unclassified. Each paragraph of the abstract shall begin with an indication of the
security classification of the information in the paragraph (unless the document itself is unclassified) represented as (S), (C), (R), or (U).
It is not necessary to include here abstracts in both official languages unless the text is bilingual).

(U)   A statistical analysis on the output signals of an acousto-optic spectrum analyzer
(AOSA) is performed for the case when the input signal is a continuous-wave (CW). To this
end, a statistical model of these output signals is presented as a basis for the different
analyses along with some numerical algorithms to calculate the deterministic components
on a digital computer.

(U)   Using this model, the optimum test for the detection of a known frequency is derived
and its performance is analyzed. To deal with the unknown frequency situation, a scheme
which is easily implemented with a finite impulse response (FIR) filter is presented and
its performance degradation as compared to the case of a known frequency is analyzed..

(U)   The frequency estimation problem is also analyzed and the Cramér-Rao lower bound on
the variance of any unbiased estimator is calculated. Since the Cramér-Rao bound indicates
that any unbiased estimator would exhibit undesirable characteristics, the performance of
the peak-detecting estimator is analyzed. It is shown that this latter estimator is
biased but has the desired characteristic of having a zero average bias.

(U)   Finally, the power estimation problem is analyzed under the assumption that the
frequency of the input signal is known. Under this assumption, it is found that the
maximum likelihood (ML) estimator is an efficient estimator which means that its variance
is the lowest possible variance of any unbiased estimator. The effects of inaccuracies
in the frequency assumption on the performance of the ML estimator are also analyzed.

14. KEYWORDS, DESCRIPTORS or IDENTIFIERS (technically meaningful terms or short phrases that characterize a document and could be
helpful in cataloguing the document. They should be selected so that no security classification is required. Identifiers, such as equipment
mode designation, trade name, military project code name, geographic location may also be included. If possible keywords should be selected
from a published thesaurus. e.g. Thesaurus of Engineering and Scientific Terms (TEST) and that thesaurus-identified. If it is not possible to
select indexing terms which are Unclassified, the classification of each should be indicated as with the title.)

Signal Processing,   ELEC—...   WAR...RE,   Radio, countermeasures,
Acousto-Optic,
Spectrum Analyzer,
Statistical Analysis,
Detection,
Estimation, CANADA,
Modelling. (TCS)

UNCLASSIFIED

SECURITY CLASSIFICATION OF FORM